An augmented velocity-vorticity-pressure formulation for the Brinkman problem*

Verónica Anaya† Gabriel N. Gatica‡
David Mora§ Ricardo Ruiz-Baier¶

Abstract

This paper deals with the analysis of a new augmented mixed finite element method in terms of vorticity, velocity and pressure, for the Brinkman problem with non-standard boundary conditions. The approach is based on the introduction of Galerkin least-squares terms arising from the constitutive equation relating the aforementioned unknowns, and from the incompressibility condition. We show that the resulting augmented bilinear form is continuous and elliptic which, thanks to the Lax-Milgram Theorem, and besides proving the well-posedness of the continuous formulation, ensures the solvability and stability of the Galerkin scheme with any finite element subspace of the continuous space. In particular, Raviart-Thomas elements of any order $k \geq 0$ for the velocity field, and piecewise continuous polynomials of degree $k+1$ for both the vorticity and the pressure, can be utilized. A priori error estimates and the corresponding rates of convergence are also given here. Next, we derive two reliable and efficient residual-based a posteriori error estimators for this problem. The ellipticity of the bilinear form together with the local approximation properties of the Clément interpolation operator are the main tools for showing the reliability. In turn, inverse inequalities and the localization technique based on triangle-bubble and edge-bubble functions are utilized to show the efficiency. Finally, several numerical results illustrating the good performance of the method, confirming the properties of the estimators, and showing the behaviour of the associated adaptive algorithms, are reported.

Key words: generalized Stokes equations, Brinkman problem, vorticity-based mixed formulation, augmented scheme, finite element method, a priori error estimates, a posteriori error analysis

Mathematics subject classifications (2000): 65N30, 65N12, 76D07, 65N15

*This work was partially supported by CONICYT-Chile through FONDECYT postdoctorado No.3120197 and project 1140791, by project Inserción de Capital Humano Avanzado en la Academia No. 79112012, by DIUBB through project 120808 GI/EF, by BASAL project CMM, Universidad de Chile, by Centro de Investigación en Ingeniería Matemática (CI^{2}MA), Universidad de Concepción, by CONICYT project Anillo ACT1118 (ANANUM), and by the University of Lausanne.

†Departamento de Matemática, Facultad de Ciencias, Universidad del Bío-Bío, Casilla 5-C, Concepción, Chile, email: vanaya@ubiobio.cl

‡CI^{2}MA and Departamento de Ingeniería Matemática, Universidad de Concepción, Casilla 160-C, Concepción, Chile, email: ggatica@ci2ma.udec.cl

§CI^{2}MA, Universidad de Concepción and Departamento de Matemática, Facultad de Ciencias, Universidad del Bío-Bío, Casilla 5-C, Concepción, Chile, email: dmora@ubiobio.cl

¶Instite of Earth Sciences, Quartier UNIL-Mouline, Bâtiment Géopolis, University of Lausanne, CH-1015 Lausanne, Switzerland, e-mail: ricardo.ruizbaier@unil.ch

1 Introduction

We are interested in the numerical approximation of the velocity–vorticity–pressure formulation of the linear Brinkman (or generalized Stokes) problem, typically encountered after time discretizations of transient Stokes equations governing the motion of an incompressible fluid. Many numerical methods have been introduced for the generalized Stokes problem in the last few years, most of them based on mixed finite element formulations and making extensive use of diverse stabilization techniques. In particular, a continuous penalty method has been proposed and analyzed in [11]. Also, a pressure gradient stabilization method for the generalized Stokes problem has been introduced in [39]. In the context of mixed finite elements, we cite [12], where a variational formulation that can be recast as a twofold saddle point problem is introduced and analyzed. The approach in [12] is based on the introduction of the flux and the tensor gradient of the velocity as further unknowns. The discrete method is based on Raviart–Thomas spaces of order zero to approximate the flux and piecewise constant functions to approximate the velocity and the pressure. In that contribution the authors prove that the continuous and discrete formulations are well-posed, and derive the associated a priori error analysis and a posteriori error estimates based on local problems. In [36], the pseudostress and the trace-free velocity gradient are introduced as auxiliary unknowns and a pseudostress-velocity formulation is considered, for which existence, uniqueness, and error estimates are derived. More recently, dual-mixed methods based on the velocity-pseudostress and pseudostress have been introduced in [4] and [27], respectively, for the generalized Stokes problem. In the former, the approach from [30] (see also [31]) is adapted to propose an augmented mixed method in terms of velocity and pseudostress, for which optimal error estimates are proved. On the other hand, in [27], a formulation based only on the pseudostress is proposed for the Brinkman problem, thus simplifying and improving the analysis from [4]. The results in [27] include a priori and a posteriori error analyses of the resulting Galerkin scheme. A considerable amount of methods have been introduced for the numerical study of the Stokes and Navier–Stokes equations formulated in terms of vorticity-velocity-pressure fields. We mention for instance, formulations based on least-squares, stabilization techniques, mixed methods, spectral discretizations, hybridizable discontinuous Galerkin, that can be found in [1, 2, 7, 9, 19, 14, 17, 18, 40, 41], and the references in these papers. However, up to our knowledge, the Brinkman problem has been considered using mixed vorticity-velocity-pressure formulations only very recently [42], in where a dual mixed formulation has been introduced and analyzed at the continuous and discrete levels using the Babuška-Brezzi theory. In particular, optimal error estimates are proved in [42].

The so-called augmented mixed finite elements (also known as Galerkin least-squares methods [9, 10, 22]) can be regarded as a stabilization technique where some terms are added to the variational formulation so that, either the resulting augmented variational formulations are defined by strongly coercive bilinear forms (see, e.g. [24]), or they enable to bypass the kernel property, which is very difficult to obtain in practice, or they allow the fulfillment of the inf-sup condition at the continuous and discrete levels in mixed formulations (see [25]). This approach has been considered in e.g. [3, 4, 29, 20, 21, 26, 35] for Stokes, generalized Stokes (in velocity-pseudostress formulation), coupling of quasi-Newtonian fluids and porous media, and Navier-Stokes equations, and in [5] for an augmented mixed formulation applied to elliptic problems with mixed boundary conditions.

In this article, we propose a new class of stabilized finite element approximations of the Brinkman equations, written in terms of the velocity, vorticity and pressure fields. One of the main goals of the present approach is to build different families of finite elements to approximate the model problem with the liberty of choosing any combination of the finite element subspaces of the continuous spaces, and extend recent results given in [3], where a new stabilized finite element approximation for the Stokes equations was analyzed using an *extension* of the Babuška-Brezzi theory (cf. [23, 28]). The

proposed method also exhibits the advantage that the vorticity unknown (which is a sought quantity of practical interest in several industrial applications) can be accessed directly, with the desired accuracy, and without the need of postprocessing. This appears to be quite difficult in mixed methods written only in terms of vector potential-vorticity (see e.g. [18, 33]).

The variational formulation is based on the introduction of suitable Galerkin least-squares terms which let us analyze the problem by the classical Lax-Milgram theorem. Indeed, to ensure the existence and uniqueness of solution, at continuous and discrete levels, we prove that the corresponding resulting augmented bilinear form is continuous and elliptic. For the numerical approximation, we consider in particular the family of finite elements $\mathbf{RT}_k - P_{k+1} - P_{k+1}$, $k \geq 0$, i.e., Raviart-Thomas elements of order k for the velocity field, piecewise continuous polynomials of degree $k+1$ for the (scalar) vorticity and the pressure. We emphasize that the present approach extends for approximations of the pressure lying *in any subspace* of $\mathrm{H}^1(\Omega)$, which differs from the mixed method in [42] where the inf-sup condition needed for the stability of the corresponding Galerkin scheme only holds for certain subspaces of $\mathrm{L}^2(\Omega)$. Numerical experiments with the family of finite elements considered in this paper perform satisfactorily for a variety of boundary conditions. We also test the applicability of the present framework using the family of finite elements: $\mathbf{BDM}_{k+1} - P_{k+1} - P_{k+1}$, $k \geq 0$ i.e., classical Brezzi-Douglas-Marini finite elements for the velocity field, and piecewise continuous polynomials of degree $k+1$ for the vorticity and the pressure. Certainly, as supported by the theory, one could employ any triple of finite element subspaces of the corresponding continuous spaces.

Outline

We have organized the contents of this paper as follows. In the remainder of this section we introduce some standard notation and needed functional spaces, describe the boundary value problem of interest, and present the associate dual mixed variational formulation which will be modified to write our method. In Section 2, we set the stabilized variational formulation, and then show that it is well-posed using the classical Lax-Milgram theorem. In Section 3, we present the discrete method, provide particular families of stable finite elements, and we obtain error estimates for the proposed methods. Section 4 is devoted to the reliability and efficiency analysis of two a posteriori error estimators. Finally, several numerical results assessing the performance of the methods, illustrating the convergence rates predicted by the theory, confirming the properties of the a posteriori error estimators, and showing the behaviour of the associated adaptive algorithms, are collected in Section 5.

Preliminaries

Let us assume that $\Omega \subset \mathbb{R}^2$ is a bounded and simply connected Lipschitz domain. We denote by $\boldsymbol{n} = (n_i)_{1\leq i\leq 2}$ the outward unit normal vector to the boundary $\Gamma := \partial\Omega$, and by $\boldsymbol{t} = (t_i)_{1\leq i\leq 2}$ the unit tangent vector to $\partial\Omega$ oriented such that $t_1 = -n_2$, $t_2 = n_1$. Moreover, we assume that $\partial\Omega$ is polygonal and admits a disjoint partition $\partial\Omega = \Gamma \cup \Sigma$. For the sake of simplicity, we also assume that both Γ and Σ have positive measure.

For $s \geq 0$, the symbol $\|\cdot\|_{s,\Omega}$ stands for the norm of the Hilbertian Sobolev spaces $\mathrm{H}^s(\Omega)$ or $\mathbf{H}^s(\Omega) = [\mathrm{H}^s(\Omega)]^2$, with the convention $\mathrm{H}^0(\Omega) := \mathrm{L}^2(\Omega)$ and $\mathbf{H}^0(\Omega) = \mathbf{L}^2(\Omega)$. We also define the Hilbert space

$$\mathbf{H}(\mathrm{div};\Omega) := \left\{ \boldsymbol{v} \in \mathbf{L}^2(\Omega) : \quad \mathrm{div}\, \boldsymbol{v} \in \mathrm{L}^2(\Omega) \right\},$$

whose norm is given by $\|\boldsymbol{v}\|^2_{\mathrm{div},\Omega} := \|\boldsymbol{v}\|^2_{0,\Omega} + \|\mathrm{div}\, \boldsymbol{v}\|^2_{0,\Omega}$. Hereafter, we use the following notation for

any vector field $\boldsymbol{v} = (v_i)_{i=1,2}$ and any scalar field η:

$$\operatorname{div}\boldsymbol{v} := \partial_1 v_1 + \partial_2 v_2, \qquad \operatorname{rot}\boldsymbol{v} := \partial_1 v_2 - \partial_2 v_1, \qquad \nabla\eta := \begin{pmatrix} \partial_1\eta \\ \partial_2\eta \end{pmatrix}, \qquad \mathbf{curl}\,\eta := \begin{pmatrix} \partial_2\eta \\ -\partial_1\eta \end{pmatrix}.$$

In addition, we will denote with c and C, with or without subscripts, tildes, or hats, a generic constant independent of the mesh parameter h, which may take different values in different occurrences.

The model problem

The Brinkman (or generalized Stokes) problem [4, 11, 27], formulated in terms of the velocity $\boldsymbol{u}$, vorticity ω and pressure p of an incompressible viscous fluid (see also [42]) reads: Given a force density $\boldsymbol{f}$, vector fields $\boldsymbol{a}$ and $\boldsymbol{b}$, and scalar fields p_0 and ω_0, we seek a vector field $\boldsymbol{u}$, a scalar field ω and a scalar field p such that

$$\left\{\begin{array}{rcll} \sigma\boldsymbol{u} + \nu\,\mathbf{curl}\,\omega + \nabla p &=& \boldsymbol{f} & \text{in } \Omega, \\ \omega - \operatorname{rot}\boldsymbol{u} &=& 0 & \text{in } \Omega, \\ \operatorname{div}\boldsymbol{u} &=& 0 & \text{in } \Omega, \\ \boldsymbol{u}\cdot\boldsymbol{t} &=& \boldsymbol{a}\cdot\boldsymbol{t} & \text{on } \Sigma, \\ p &=& p_0 & \text{on } \Sigma, \\ \boldsymbol{u}\cdot\boldsymbol{n} &=& \boldsymbol{b}\cdot\boldsymbol{n} & \text{on } \Gamma, \\ \omega &=& \omega_0 & \text{on } \Gamma, \end{array}\right. \tag{1.1}$$

where $\boldsymbol{u}\cdot\boldsymbol{t}$ and $\boldsymbol{u}\cdot\boldsymbol{n}$ stand for the normal and tangential components of the velocity, respectively. In the model, $\nu > 0$ is the kinematic viscosity of the fluid and $\sigma > 0$ is a parameter proportional to the inverse of the time-step. In addition, we assume that a *boundary compatibility condition* holds, i.e., there exists a velocity field $\boldsymbol{w} \in \mathrm{L}^2(\Omega)^2$ satisfying $\operatorname{div}\boldsymbol{w} = 0$ a.e. in Ω, $\boldsymbol{w}\cdot\boldsymbol{t} = \boldsymbol{a}\cdot\boldsymbol{t}$ on Σ, and $\boldsymbol{w}\cdot\boldsymbol{n} = \boldsymbol{b}\cdot\boldsymbol{n}$ on Γ. For a detailed study on different types of standard and non-standard boundary conditions for incompressible flows we refer to [8, 37]. We observe that the boundary conditions considered here are relevant, for instance, in the context of geophysical fluids and shallow water models [38].

For the sake of simplicity, throughout the rest of the paper we assume homogeneous boundary conditions for the pressure, normal velocity, and vorticity, i.e., $p_0 = 0$ on Σ, $\boldsymbol{b} = \boldsymbol{0}$ on Γ, and $\omega_0 = 0$ on Γ.

2 The augmented vorticity-velocity-pressure formulation

2.1 Variational formulations and preliminary results

In this section, we set the dual-mixed variational formulation of problem (1.1), and then propose a corresponding augmented approach. To this end, we first introduce the spaces

$$\mathbf{H}_\Gamma(\operatorname{div};\Omega) := \{\boldsymbol{v} \in \mathbf{H}(\operatorname{div};\Omega) : \quad \boldsymbol{v}\cdot\boldsymbol{n} = 0 \text{ on } \Gamma\} \quad \text{and} \quad \mathrm{H}^1_\Gamma(\Omega) := \{\eta \in \mathrm{H}^1(\Omega) : \quad \eta = 0 \text{ on } \Gamma\},$$

which are endowed with the natural norms, and denote by $\langle\cdot,\cdot\rangle_\Sigma$ the duality pairing between $\mathrm{H}^{-1/2}(\Sigma)$ and $\mathrm{H}^{1/2}(\Sigma)$ with respect to the $\mathrm{L}^2(\Sigma)$-inner product. Then, by testing system (1.1) with adequate functions and imposing the boundary conditions, we obtain the following dual-mixed variational for-

mulation: *Find* $(\boldsymbol{u},\omega,p)\in \mathbf{H}_\Gamma(\mathrm{div};\Omega)\times \mathrm{H}^1_\Gamma(\Omega)\times \mathrm{L}^2(\Omega)$ *such that*

$$\begin{aligned}
\sigma\int_\Omega \boldsymbol{u}\cdot\boldsymbol{v}+\nu\int_\Omega \mathbf{curl}\,\omega\cdot\boldsymbol{v}-\int_\Omega p\,\mathrm{div}\,\boldsymbol{v} &= \int_\Omega \boldsymbol{f}\cdot\boldsymbol{v} && \forall \boldsymbol{v}\in \mathbf{H}_\Gamma(\mathrm{div};\Omega)\,,\\
\nu\int_\Omega \mathbf{curl}\,\eta\cdot\boldsymbol{u}-\nu\int_\Omega \omega\eta &= -\nu\langle \boldsymbol{a}\cdot\boldsymbol{t},\eta\rangle_\Sigma && \forall \eta\in \mathrm{H}^1_\Gamma(\Omega)\,, \qquad (2.1)\\
-\int_\Omega q\,\mathrm{div}\,\boldsymbol{u} &= 0 && \forall q\in \mathrm{L}^2(\Omega)\,.
\end{aligned}$$

Note that this variational problem can be rewritten as a twofold saddle point problem (cf. [23, 28]): *Find* $(\boldsymbol{u},\omega,p)\in \mathbf{H}_\Gamma(\mathrm{div};\Omega)\times \mathrm{H}^1_\Gamma(\Omega)\times \mathrm{L}^2(\Omega)$ *such that*

$$\begin{aligned}
a(\boldsymbol{u},\boldsymbol{v})+b_1(\boldsymbol{v},\omega)+b_2(p,\boldsymbol{v}) &= G(\boldsymbol{v}) && \forall \boldsymbol{v}\in \mathbf{H}_\Gamma(\mathrm{div};\Omega),\\
b_1(\boldsymbol{u},\eta)-d(\omega,\eta) &= F(\eta) && \forall \eta\in \mathrm{H}^1_\Gamma(\Omega), \qquad (2.2)\\
b_2(q,\boldsymbol{u}) &= 0 && \forall q\in \mathrm{L}^2(\Omega)\,,
\end{aligned}$$

where the bilinear forms $a:\mathbf{H}_\Gamma(\mathrm{div};\Omega)\times\mathbf{H}_\Gamma(\mathrm{div};\Omega)\to\mathbb{R}$, $b_1:\mathbf{H}_\Gamma(\mathrm{div};\Omega)\times\mathrm{H}^1_\Gamma(\Omega)\to\mathbb{R}$, $b_2:\mathrm{L}^2(\Omega)\times\mathbf{H}_\Gamma(\mathrm{div};\Omega)\to\mathbb{R}$, $d:\mathrm{H}^1_\Gamma(\Omega)\times\mathrm{H}^1_\Gamma(\Omega)\to\mathbb{R}$, and the linear functionals $G:\mathbf{H}_\Gamma(\mathrm{div};\Omega)\to\mathbb{R}$, and $F:\mathrm{H}^1_\Gamma(\Omega)\to\mathbb{R}$ are defined by

$$\begin{aligned}
a(\boldsymbol{u},\boldsymbol{v}) &:= \sigma\int_\Omega \boldsymbol{u}\cdot\boldsymbol{v}, \qquad & b_1(\boldsymbol{v},\eta) &:= \nu\int_\Omega \mathbf{curl}\,\eta\cdot\boldsymbol{v},\\
d(\omega,\eta) &:= \nu\int_\Omega \omega\eta, \qquad & b_2(q,\boldsymbol{v}) &:= -\int_\Omega q\,\mathrm{div}\,\boldsymbol{v},
\end{aligned}$$

and

$$G(\boldsymbol{v}) := \int_\Omega \boldsymbol{f}\cdot\boldsymbol{v}\,, \qquad F(\eta) := -\nu\langle \boldsymbol{a}\cdot\boldsymbol{t},\eta\rangle_\Sigma,$$

for all $\boldsymbol{u},\boldsymbol{v}\in\mathbf{H}_\Gamma(\mathrm{div};\Omega)$, $\omega,\eta\in\mathrm{H}^1_\Gamma(\Omega)$, and $q\in\mathrm{L}^2(\Omega)$.

The well-posedness of (2.2) has been recently proved in [42]. In turn, the converse of the derivation of (2.2) is provided next. More precisely, the following theorem establishes that the unique solution of (2.2) solves the original boundary value problem (1.1).

Theorem 2.1. *Let* $(\boldsymbol{u},\omega,p)\in\mathbb{H}$ *be the unique solution of* (2.2). *Then* $\mathrm{div}\,\boldsymbol{u}=0$ *in* Ω, $\omega=\mathrm{rot}\,\boldsymbol{u}$ *in* Ω, $\boldsymbol{u}\cdot\boldsymbol{t}=\boldsymbol{a}\cdot\boldsymbol{t}$ *on* Σ, $\sigma\,\boldsymbol{u}+\nu\,\mathbf{curl}\,\omega+\nabla p=\boldsymbol{f}$ *in* Ω (*which yields* $p\in H^1(\Omega)$), *and* $p=0$ *on* Σ.

Proof. It follows by integrating backwardly in (2.2) and employing suitable test functions. Further details are omitted. □

Now, since p actually lives in the space $\mathrm{H}^1(\Omega)$, we suggest to enrich the above system (2.1) with residuals arising from the first and the third equations of system (1.1). This approach permits us to analyze the problem directly under the classical Lax-Milgram theorem. More precisely, we add to the system (2.1) the following Galerkin least-squares terms:

$$\begin{aligned}
\kappa_1\int_\Omega(\sigma\boldsymbol{u}+\nu\,\mathbf{curl}\,\omega+\nabla p-\boldsymbol{f})\cdot\mathbf{curl}\,\eta &= 0 && \forall \eta\in\mathrm{H}^1_\Gamma(\Omega)\,,\\
\kappa_2\int_\Omega(\sigma\boldsymbol{u}+\nu\,\mathbf{curl}\,\omega+\nabla p-\boldsymbol{f})\cdot\nabla q &= 0 && \forall q\in\mathrm{H}^1_\Sigma(\Omega)\,, \qquad (2.3)\\
\kappa_3\int_\Omega \mathrm{div}\,\boldsymbol{u}\,\mathrm{div}\,\boldsymbol{v} &= 0 && \forall \boldsymbol{v}\in\mathbf{H}_\Gamma(\mathrm{div};\Omega)\,,
\end{aligned}$$

where κ_1, κ_2 and κ_3 are positive stabilization parameters to be specified later, and

$$\mathrm{H}^1_\Sigma(\Omega) := \{q \in \mathrm{H}^1(\Omega) : \quad q = 0 \text{ on } \Sigma\},$$

Using an integration by parts, the fact that $\operatorname{div}\mathbf{curl}$ is the null operator, and the boundary conditions, we may rewrite the first two equations of (2.3) equivalently as follows:

$$\kappa_1\sigma\int_\Omega \boldsymbol{u}\cdot\mathbf{curl}\,\eta + \kappa_1\nu\int_\Omega \mathbf{curl}\,\omega\cdot\mathbf{curl}\,\eta = \kappa_1\int_\Omega \boldsymbol{f}\cdot\mathbf{curl}\,\eta \qquad \forall \eta\in \mathrm{H}^1_\Gamma(\Omega),$$
$$\kappa_2\sigma\int_\Omega \boldsymbol{u}\cdot\nabla q + \kappa_2\int_\Omega \nabla p\cdot\nabla q = \kappa_2\int_\Omega \boldsymbol{f}\cdot\nabla q \qquad \forall q\in \mathrm{H}^1_\Sigma(\Omega).$$

In this way, we propose the following augmented variational formulation: *Find* $\vec{\boldsymbol{u}} := (\boldsymbol{u},\omega,p)\in\mathbb{H}$ *such that*

$$\mathcal{A}(\vec{\boldsymbol{u}},\vec{\boldsymbol{v}}) = \mathcal{G}(\vec{\boldsymbol{v}}) \qquad \forall\,\vec{\boldsymbol{v}} := (\boldsymbol{v},\eta,q)\in\mathbb{H}, \tag{2.4}$$

where the space $\mathbb{H} := \mathbf{H}_\Gamma(\operatorname{div};\Omega)\times \mathrm{H}^1_\Gamma(\Omega)\times \mathrm{H}^1_\Sigma(\Omega)$ is endowed with the corresponding product norm, and the bilinear form $\mathcal{A}:\mathbb{H}\times\mathbb{H}\to\mathbb{R}$ and the linear functional $\mathcal{G}:\mathbb{H}\to\mathbb{R}$ are defined by

$$\begin{aligned}\mathcal{A}(\vec{\boldsymbol{u}},\vec{\boldsymbol{v}}) \;:=\; & \sigma\int_\Omega \boldsymbol{u}\cdot\boldsymbol{v} + \nu\int_\Omega \mathbf{curl}\,\omega\cdot\boldsymbol{v} - \int_\Omega p\operatorname{div}\boldsymbol{v} - \nu\int_\Omega \mathbf{curl}\,\eta\cdot\boldsymbol{u} + \nu\int_\Omega \omega\eta \\ + \quad & \int_\Omega q\operatorname{div}\boldsymbol{u} + \kappa_1\sigma\int_\Omega \boldsymbol{u}\cdot\mathbf{curl}\,\eta + \kappa_1\nu\int_\Omega \mathbf{curl}\,\omega\cdot\mathbf{curl}\,\eta + \kappa_2\sigma\int_\Omega \boldsymbol{u}\cdot\nabla q \\ + \quad & \kappa_2\int_\Omega \nabla p\cdot\nabla q + \kappa_3\int_\Omega \operatorname{div}\boldsymbol{u}\operatorname{div}\boldsymbol{v},\end{aligned} \tag{2.5}$$

and

$$\mathcal{G}(\vec{\boldsymbol{v}}) := \int_\Omega \boldsymbol{f}\cdot\boldsymbol{v} + \nu\langle \boldsymbol{a}\cdot\boldsymbol{t},\eta\rangle_\Sigma + \kappa_1\int_\Omega \boldsymbol{f}\cdot\mathbf{curl}\,\eta + \kappa_2\int_\Omega \boldsymbol{f}\cdot\nabla q, \tag{2.6}$$

for all $\vec{\boldsymbol{u}} := (\boldsymbol{u},\omega,p)$, $\vec{\boldsymbol{v}} := (\boldsymbol{v},\eta,q)\in\mathbb{H}$.

2.2 Unique solvability of the augmented formulation

Next, we will prove that our augmented variational formulation (2.4) satisfies the hypotheses of the Lax-Milgram theorem, i.e., the idea is to choose κ_1,κ_2 and κ_3 so that the bilinear form $\mathcal{A}$ becomes strongly coercive on $\mathbb{H}$, which yields the unique solvability and continuous dependence on the data of this variational formulation. First, we observe that the bilinear form $\mathcal{A}$, and the linear functional $\mathcal{G}$ are bounded. More precisely, there exist C_1, $C_2>0$ such that

$$\begin{aligned} |\mathcal{A}(\vec{\boldsymbol{w}},\vec{\boldsymbol{v}})| &\le C_1\|\vec{\boldsymbol{w}}\|_{\mathbb{H}}\,\|\vec{\boldsymbol{v}}\|_{\mathbb{H}} && \forall\,\vec{\boldsymbol{w}},\,\boldsymbol{v}\in\mathbb{H}, \\ |\mathcal{G}(\vec{\boldsymbol{v}})| &\le C_2\left\{\|\boldsymbol{a}\cdot\boldsymbol{t}\|_{-1/2,\Sigma} + \|\boldsymbol{f}\|_{0,\Omega}\right\}\|\vec{\boldsymbol{v}}\|_{\mathbb{H}} && \forall\,\vec{\boldsymbol{v}}\in\mathbb{H}. \end{aligned} \tag{2.7}$$

The following lemma shows that the bilinear form $\mathcal{A}$ is $\mathbb{H}-$elliptic.

Lemma 2.2. *Assume that* $\kappa_1\in(0,\frac{\nu}{\sigma})$, $\kappa_2\in(0,\frac{1}{\sigma})$, *and* $\kappa_3>0$. *Then, there exists* $\alpha>0$ *such that*

$$\mathcal{A}(\vec{\boldsymbol{v}},\vec{\boldsymbol{v}}) \;\ge\; \alpha\,\|\vec{\boldsymbol{v}}\|^2_{\mathbb{H}} \qquad \forall\,\vec{\boldsymbol{v}}\in\mathbb{H}.$$

Proof. According to the definition of $\mathcal{A}$ in (2.5) and applying the Cauchy-Schwarz inequality, we obtain

$$\begin{aligned}\mathcal{A}(\vec{\boldsymbol{v}},\vec{\boldsymbol{v}}) &= \sigma\|\boldsymbol{v}\|^2_{0,\Omega}+\nu\|\eta\|^2_{0,\Omega}+\kappa_1\sigma\int_\Omega \mathbf{curl}\,\eta\cdot\boldsymbol{v}+\kappa_1\nu|\eta|^2_{1,\Omega}+\kappa_2\sigma\int_\Omega \boldsymbol{v}\cdot\nabla q+\kappa_2|q|^2_{1,\Omega}+\kappa_3\|\operatorname{div}\boldsymbol{v}\|^2_{0,\Omega}\\ &\geq \sigma\|\boldsymbol{v}\|^2_{0,\Omega}+\nu\|\eta\|^2_{0,\Omega}-\kappa_1\sigma|\eta|_{1,\Omega}\|\boldsymbol{v}\|_{0,\Omega}+\kappa_1\nu|\eta|^2_{1,\Omega}-\kappa_2\sigma\|\boldsymbol{v}\|_{0,\Omega}|q|_{1,\Omega}+\kappa_2|q|^2_{1,\Omega}+\kappa_3\|\operatorname{div}\boldsymbol{v}\|^2_{0,\Omega}\end{aligned}$$

Next, employing the inequality $ab \leq a^2 + \frac{1}{4}b^2$, we find that

$$\kappa_1\sigma|\eta|_{1,\Omega}\|\boldsymbol{v}\|_{0,\Omega} \leq \kappa_1^2\sigma|\eta|^2_{1,\Omega}+\frac{\sigma}{4}\|\boldsymbol{v}\|^2_{0,\Omega} \quad\text{and}\quad \kappa_2\sigma\|\boldsymbol{v}\|_{0,\Omega}|q|_{1,\Omega} \leq \kappa_2^2\sigma|q|^2_{1,\Omega}+\frac{\sigma}{4}\|\boldsymbol{v}\|^2_{0,\Omega},$$

which, together with the previous inequality, yields

$$\begin{aligned}\mathcal{A}(\vec{\boldsymbol{v}},\vec{\boldsymbol{v}}) &\geq \frac{\sigma}{2}\|\boldsymbol{v}\|^2_{0,\Omega}+\nu\|\eta\|^2_{0,\Omega}-\kappa_1^2\sigma|\eta|^2_{1,\Omega}+\kappa_1\nu|\eta|^2_{1,\Omega}-\kappa_2^2\sigma|q|^2_{1,\Omega}+\kappa_2|q|^2_{1,\Omega}+\kappa_3\|\operatorname{div}\boldsymbol{v}\|^2_{0,\Omega}\\ &\geq \min\left\{\frac{\sigma}{2},\kappa_3\right\}\|\boldsymbol{v}\|^2_{\mathrm{div},\Omega}+\nu\|\eta\|^2_{0,\Omega}+\kappa_1(\nu-\kappa_1\sigma)|\eta|^2_{1,\Omega}+\kappa_2(1-\kappa_2\sigma|q|^2_{1,\Omega}.\end{aligned}$$

Finally, the proof is completed by straightforward applications of the Poincaré inequality. □

We are now in a position to state the main result of this section which yields the solvability of the continuous formulation (2.4).

Theorem 2.3. *Assume the same hypotheses of Lemma 2.2. Then, formulation* (2.4) *admits a unique solution* $\vec{\boldsymbol{u}} := (\boldsymbol{u},\omega,p) \in \mathbb{H}$. *Moreover, there exists* $C>0$ *such that*

$$\|\vec{\boldsymbol{u}}\|_{\mathbb{H}} \leq C\left\{\|\boldsymbol{a}\cdot\boldsymbol{t}\|_{-1/2,\Sigma}+\|\boldsymbol{f}\|_{0,\Omega}\right\}.$$

Proof. The bilinear form $\mathcal{A}$ and the linear functional $\mathcal{G}$ are continuous (see (2.7)). Hence, the proof is a simple consequence of Lemma 2.2 and the well-known Lax-Milgram theorem. □

It is important to remark at this point that the unique solution of (2.2) is certainly solution of (2.4), and hence, since the latter is also uniquely solvable, it is clear that the solutions of both problems coincide. This means, in particular, that Theorem 2.1 is obviously valid for the solution $\vec{\boldsymbol{u}} := (\boldsymbol{u},\omega,p)$ of (2.4) as well. This fact is employed later on in Section 4 to prove the efficiency of the a posteriori error estimators derived previously in that section.

3 The augmented finite element scheme

In this section, we construct a finite element scheme associated to (2.4), define explicit finite element subspaces yielding the unique solvability of the discrete schemes, derive the a priori error estimates, and provide the rate of convergence of the methods. Let $\mathcal{T}_h$ be a regular family of triangulations of the polygonal region $\bar{\Omega}$ by triangles T of diameter h_T with mesh size $h := \max\{h_T : T \in \mathcal{T}_h\}$, and such that there holds $\bar{\Omega} = \cup\{T : T \in \mathcal{T}_h\}$. In addition, given an integer $k \geq 0$ and a subset S of $\mathbb{R}^2$, we denote by $P_k(S)$ the space of polynomials in two variables defined in S of total degree at most k and we write $\mathbf{P}_k(S) = [P_k(S)]^2$. By $\mathbf{RT}_k(T)$ we will denote the local Raviart-Thomas space of order k defined as usual

$$\mathbf{RT}_k(T) := \mathbf{P}_k(T) \oplus P_k(T)\boldsymbol{x},$$

with $\boldsymbol{x}$ being a generic vector of $\mathbb{R}^2$. In addition, we let $\mathbf{RT}_k(\Omega)$ be the global Raviart-Thomas space of order k, that is

$$\mathbf{RT}_k(\Omega) := \Big\{ \boldsymbol{v}_h \in \mathbf{H}(\mathrm{div};\Omega) : \quad \boldsymbol{v}_h|_T \in \mathbf{RT}_k(T) \quad \forall\, T \in \mathcal{T}_h \Big\}. \tag{3.1}$$

Now, given finite element subspaces $\mathbf{H}_h^{\boldsymbol{u}} \subset \mathbf{H}_\Gamma(\mathrm{div};\Omega)$, $\mathrm{H}_h^{\omega} \subset \mathrm{H}^1_\Gamma(\Omega)$ and $\mathrm{H}_h^{p} \subset \mathrm{H}^1_\Sigma(\Omega)$, the Galerkin scheme associated with the continuous variational formulation (2.4) reads as follows: *Find* $\vec{\boldsymbol{u}}_h := (\boldsymbol{u}_h, \omega_h, p_h) \in \mathbb{H}_h$ *such that*

$$\mathcal{A}(\vec{\boldsymbol{u}}_h, \vec{\boldsymbol{v}}_h) \,=\, \mathcal{G}(\vec{\boldsymbol{v}}_h) \qquad \forall\, \vec{\boldsymbol{v}}_h \,:=\, (\boldsymbol{v}_h, \eta_h, q_h) \in \mathbb{H}_h\,, \tag{3.2}$$

where the space $\mathbb{H}_h := \mathbf{H}_h^{\boldsymbol{u}} \times \mathrm{H}_h^{\omega} \times \mathrm{H}_h^{p}$, and κ_1, κ_2 and κ_3 are the same parameters employed in the continuous formulation (2.4).

Since the bilinear form $\mathcal{A}$ is bounded and strongly coercive on the whole space $\mathbb{H}$ (see Theorem 2.3), the well-posedness of (3.2) is guaranteed with any arbitrary choice of the subspace $\mathbb{H}_h$. In particular, we define the following finite element subspaces for $k \geq 0$:

$$\mathbf{H}_h^{\boldsymbol{u}} := \mathbf{H}_\Gamma(\mathrm{div};\Omega) \cap \mathbf{RT}_k(\Omega) \,=\, \{\boldsymbol{v}_h \in \mathbf{H}_\Gamma(\mathrm{div};\Omega) : \quad \boldsymbol{v}_h|_T \in \mathbf{RT}_k(T) \quad \forall\, T \in \mathcal{T}_h\}, \tag{3.3}$$

$$\tilde{\mathbf{H}}_h^{\boldsymbol{u}} := \{\boldsymbol{v}_h \in \mathbf{H}_\Gamma(\mathrm{div};\Omega) : \quad \boldsymbol{v}_h|_T \in \mathbf{P}_{k+1}(T) \quad \forall\, T \in \mathcal{T}_h\}, \tag{3.4}$$

$$\mathrm{H}_h^{\omega} := \big\{\eta_h \in \mathrm{H}^1_\Gamma(\Omega) : \quad \eta_h|_T \in P_{k+1}(T) \quad \forall\, T \in \mathcal{T}_h\big\}\,, \tag{3.5}$$

$$\mathrm{H}_h^{p} := \{q_h \in \mathrm{H}^1_\Sigma(\Omega) : \quad q_h|_T \in P_{k+1}(T) \quad \forall\, T \in \mathcal{T}_h\}\,, \tag{3.6}$$

Notice that $\tilde{\mathbf{H}}_h^{\boldsymbol{u}}$ is the component of the Brezzi-Douglas-Marini finite element space approximating $\boldsymbol{u}$. According to the above, we may consider the following families of finite elements: $\mathbb{H}_h := \mathbf{H}_h^{\boldsymbol{u}} \times \mathrm{H}_h^{\omega} \times \mathrm{H}_h^{p}$ or $\mathbb{H}_h := \tilde{\mathbf{H}}_h^{\boldsymbol{u}} \times \mathrm{H}_h^{\omega} \times \mathrm{H}_h^{p}$.

In general, we have the following main result which establishes the unique solvability, and some convergence properties of the discrete problem (3.2).

Theorem 3.1. *Assume that* $\kappa_1 \in (0, \frac{\nu}{\sigma})$, $\kappa_2 \in (0, \frac{1}{\sigma})$, *and* $\kappa_3 > 0$, *and let* $\mathbb{H}_h$ *be any finite element subspace of* $\mathbb{H}$. *Then, the discrete formulation* (3.2) *admits a unique solution* $\vec{\boldsymbol{u}}_h \in \mathbb{H}_h$. *Moreover, there exist* $\widehat{C}, \widetilde{C} > 0$ *such that*

$$\|\vec{\boldsymbol{u}}_h\|_{\mathbb{H}} \,\leq\, \widehat{C}\,\Big\{\|\boldsymbol{a}\cdot\boldsymbol{t}\|_{-1/2,\Sigma} + \|\boldsymbol{f}\|_{0,\Omega}\Big\}\,,$$

and

$$\|\vec{\boldsymbol{u}} - \vec{\boldsymbol{u}}_h\|_{\mathbb{H}} \,\leq\, \widetilde{C} \inf_{\vec{\boldsymbol{v}}_h \in \mathbb{H}_h} \|\vec{\boldsymbol{u}} \,-\, \vec{\boldsymbol{v}}_h\|_{\mathbb{H}}\,. \tag{3.7}$$

Proof. It follows straightforward from Lemma 2.2, Lax-Milgram theorem, and the Céa estimate. □

As usual, the estimate (3.7) and the approximation properties of the subspaces considered are the key ingredients to obtain the corresponding rate of convergence of the finite element scheme (3.2). In fact, let us consider the family $\mathbb{H}_h := \mathbf{H}_h^{\boldsymbol{u}} \times \mathrm{H}_h^{\omega} \times \mathrm{H}_h^{p}$, with $\mathbf{H}_h^{\boldsymbol{u}}, \mathrm{H}_h^{\omega}$ and H_h^{p}, given in (3.3), (3.5) and (3.6), respectively. Hence, we have the following (cf. [10, 15, 25]):

($\mathrm{AP}_h^{\boldsymbol{u}}$) there exists $C > 0$, independent of h, such that for each $s \in (0, k+1]$ and for each $\boldsymbol{v} \in \mathbf{H}^s(\Omega) \cap \mathbf{H}_\Gamma(\mathrm{div};\Omega)$ with $\mathrm{div}\,\boldsymbol{v} \in \mathrm{H}^s(\Omega)$, there holds

$$\inf_{\boldsymbol{v}_h \in \mathbf{H}_h^{\boldsymbol{u}}} \|\boldsymbol{v} - \boldsymbol{v}_h\|_{\mathrm{div},\Omega} \,\leq\, C\, h^s \,\Big\{\|\boldsymbol{v}\|_{s,\Omega} \,+\, \|\mathrm{div}\,\boldsymbol{v}\|_{s,\Omega}\Big\}\,.$$

(AP_h^{ω}) there exists $C > 0$, independent of h, such that for each $s \in (0, k+1]$ and for each $\eta \in \mathrm{H}^{s+1}(\Omega)$ there holds

$$\inf_{\eta_h \in \mathrm{H}_h^{\omega}} \|\eta - \eta_h\|_{1,\Omega} \leq C\, h^s\, \|\eta\|_{s+1,\Omega}\,.$$

(AP_h^{p}) there exists $C > 0$, independent of h, such that for each $s \in (0, k+1]$ and for each $q \in \mathrm{H}^{s+1}(\Omega)$ there holds

$$\inf_{q_h \in \mathrm{H}_h^{p}} \|q - q_h\|_{1,\Omega} \leq C\, h^s\, \|q\|_{s+1,\Omega}\,.$$

The following theorem provides the rate of convergence of our finite element scheme (3.2).

Theorem 3.2. *Let k be a non-negative integer and let $\mathbf{H}_h^{\boldsymbol{u}}, \mathrm{H}_h^{\omega}$ and H_h^{p} be given by* (3.3), (3.5) *and* (3.6). *Let $\vec{\boldsymbol{u}} := (\boldsymbol{u}, \omega, p) \in \mathbb{H}$ and $\vec{\boldsymbol{u}}_h := (\boldsymbol{u}_h, \omega_h, p_h) \in \mathbb{H}_h := \mathbf{H}_h^{\boldsymbol{u}} \times \mathrm{H}_h^{\omega} \times \mathrm{H}_h^{p}$ be the unique solutions to the continuous and discrete problems* (2.4) *and* (3.2), *respectively. Assume that $\boldsymbol{u} \in \mathbf{H}^s(\Omega)$, $\operatorname{div} \boldsymbol{u} \in \mathrm{H}^s(\Omega)$, $\omega \in \mathrm{H}^{1+s}(\Omega)$, and $p \in \mathrm{H}^{1+s}(\Omega)$, for some $s \in (0, k+1]$. Then, there exists $\widehat{C} > 0$ independent of h such that*

$$\|\vec{\boldsymbol{u}} - \vec{\boldsymbol{u}}_h\|_{\mathbb{H}} \leq \widehat{C}\, h^s \left\{ \|\boldsymbol{u}\|_{s,\Omega} + \|\operatorname{div} \boldsymbol{u}\|_{s,\Omega} + \|\omega\|_{1+s,\Omega} + \|p\|_{1+s,\Omega} \right\}.$$

Proof. The proof follows from (3.7) and the approximation properties given by $(\mathrm{AP}_h^{\boldsymbol{u}})$, (AP_h^{ω}), and (AP_h^{p}). □

We remark here that if we consider the family $\mathbb{H}_h := \tilde{\mathbf{H}}_h^{\boldsymbol{u}} \times \mathrm{H}_h^{\omega} \times \mathrm{H}_h^{p}$, with $\tilde{\mathbf{H}}_h^{\boldsymbol{u}}, \mathrm{H}_h^{\omega}$ and H_h^{p}, given in (3.4), (3.5) and (3.6), respectively, to solve the problem (3.2), then the analogue of Theorem 3.2 does hold as well.

On the other hand, concerning the practical choice of the stabilization parameters κ_i, $i \in \{1, 2, 3\}$, particularly for sake of the computational implementation of the augmented mixed finite element method, we first observe that the optimal values of κ_1 and κ_2, namely those yielding the largest ellipticity constant α (cf. Lemma 2.2), are given by the midpoints of the corresponding feasible intervals, that is $\kappa_1 = \frac{\nu}{2\sigma}$ and $\kappa_2 = \frac{1}{2\sigma}$. In addition, as suggested by the first term in the last inequality of the proof of Lemma 2.2, a suitable choice for κ_3 would be given by any value $\geq \frac{\sigma}{2}$. The selections described here are employed below in Section 5.

4 A posteriori error analysis

Here we propose two alternative a posteriori error estimators and analyze their reliability and efficiency. We begin by introducing several notations. We let $\mathcal{E}_h$ be the set of all edges of the triangulation $\mathcal{T}_h$, and given $T \in \mathcal{T}_h$, we let $\mathcal{E}(T)$ be the set of its edges. Then we write $\mathcal{E}_h = \mathcal{E}_h(\Omega) \cup \mathcal{E}_h(\Gamma) \cup \mathcal{E}_h(\Sigma)$, where $\mathcal{E}_h(\Omega) := \{e \in \mathcal{E}_h : \quad e \subseteq \Omega\}$, $\mathcal{E}_h(\Gamma) := \{e \in \mathcal{E}_h : \quad e \subseteq \Gamma\}$, and analogously for $\mathcal{E}_h(\Sigma)$. In what follows, h_e stands for the length of a given edge e. Also, for each edge $e \in \mathcal{E}_h$ we fix a unit normal vector $\boldsymbol{n}_e := (n_1, n_2)^{\mathtt{t}}$, and let $\boldsymbol{t}_e := (-n_2, n_1)^{\mathtt{t}}$ be the corresponding fixed unit tangential vector along e. However, when no confusion arises, we simple write $\boldsymbol{n}$ and $\boldsymbol{t}$ instead of $\boldsymbol{n}_e$ and $\boldsymbol{t}_e$, respectively. Now, let $\boldsymbol{v} \in \mathbf{L}^2(\Omega)$ such that $\boldsymbol{v}|_T \in \mathbf{C}(T)$ on each $T \in \mathcal{T}_h$. Then, given $T \in \mathcal{T}_h$ and $e \in \mathcal{E}(T) \cap \mathcal{E}_h(\Omega)$, we denote by $[\boldsymbol{v} \cdot \boldsymbol{t}]$ and $[\boldsymbol{v} \cdot \boldsymbol{n}]$ the tangential and normal jumps of $\boldsymbol{v}$ across e, that is $[\boldsymbol{v} \cdot \boldsymbol{t}] := (\boldsymbol{v}|_T - \boldsymbol{v}|_{T'})|_e \cdot \boldsymbol{t}$ and $[\boldsymbol{v} \cdot \boldsymbol{n}] := (\boldsymbol{v}|_T - \boldsymbol{v}|_{T'})|_e \cdot \boldsymbol{n}$, where T and T' are the triangles of $\mathcal{T}_h$ having e as a common edge.

4.1 The main results

As in the previous sections, we consider $\mathbb{H}_h = \mathbf{H}_h^{\boldsymbol{u}} \times \mathrm{H}_h^{\omega} \times \mathrm{H}_h^{p}$, where, given an integer $k \geq 0$, the component subspaces are defined by (3.3), (3.5), and (3.6), respectively. Next, letting $\vec{\boldsymbol{u}}_h := (\boldsymbol{u}_h, \omega_h, p_h) \in \mathbb{H}_h$ be the unique solution of (3.2), we set the residuals

$$\mathbf{r}(\boldsymbol{u}_h, \omega_h) := \boldsymbol{f} - \sigma\, \boldsymbol{u}_h - \nu\, \mathbf{curl}\, \omega_h\,, \qquad \mathbf{r}(\boldsymbol{u}_h, p_h) := \boldsymbol{f} - \sigma\, \boldsymbol{u}_h - \nabla p_h\,,$$

and

$$\mathbf{r}(\boldsymbol{u}_h, \omega_h, p_h) := \boldsymbol{f} - \sigma\, \boldsymbol{u}_h - \nu\, \mathbf{curl}\, \omega_h - \nabla p_h\,,$$

and define for each $T \in \mathcal{T}_h$ the a posteriori error indicators

$$\begin{aligned}\theta_T^2 :=\ & \|\mathbf{r}(\boldsymbol{u}_h, \omega_h, p_h)\|_{0,T}^2 + \|\mathrm{div}\, \boldsymbol{u}_h\|_{0,T}^2 + h_T^2\, \|\,\mathrm{rot}\, \boldsymbol{u}_h - \omega_h\,\|_{0,T}^2 + h_T^2\, \|\,\mathrm{rot}\,\big\{\mathbf{r}(\boldsymbol{u}_h, \omega_h)\big\}\|_{0,T}^2 \\ &+ \sum_{e \in \mathcal{E}(T) \cap \mathcal{E}_h(\Sigma)} h_e\, \|\boldsymbol{a} \cdot \boldsymbol{t} - \boldsymbol{u}_h \cdot \boldsymbol{t}\,\|_{0,\,e}^2 + \sum_{e \in \mathcal{E}(T) \cap \mathcal{E}_h(\Omega)} h_e\, \|\,[\boldsymbol{u}_h \cdot \boldsymbol{t}]\,\|_{0,e}^2 \\ &+ \sum_{e \in \mathcal{E}(T) \cap \mathcal{E}_h(\Omega)} h_e\, \|[\mathbf{r}(\boldsymbol{u}_h, \omega_h) \cdot \boldsymbol{t}]\,\|_{0,e}^2 + \sum_{e \in \mathcal{E}(T) \cap \mathcal{E}_h(\Sigma)} h_e\, \|\mathbf{r}(\boldsymbol{u}_h, \omega_h) \cdot \boldsymbol{t}\,\|_{0,e}^2\,,\end{aligned} \tag{4.1}$$

and

$$\begin{aligned}\vartheta_T^2 :=\ & \theta_T^2 + h_T^2\, \|\mathrm{div}\,\big\{\mathbf{r}(\boldsymbol{u}_h, p_h)\big\}\|_{0,T}^2 + \sum_{e \in \mathcal{E}(T) \cap \mathcal{E}_h(\Omega)} h_e\, \|[\mathbf{r}(\boldsymbol{u}_h, p_h) \cdot \boldsymbol{n}]\,\|_{0,e}^2 \\ &+ \sum_{e \in \mathcal{E}(T) \cap \mathcal{E}_h(\Gamma)} h_e\, \|\mathbf{r}(\boldsymbol{u}_h, p_h) \cdot \boldsymbol{n}\,\|_{0,e}^2\,,\end{aligned} \tag{4.2}$$

so that the global a posteriori error estimators are given, respectively, by

$$\boldsymbol{\theta} := \left\{ \sum_{T \in \mathcal{T}_h} \theta_T^2 \right\}^{1/2} \qquad \text{and} \qquad \boldsymbol{\vartheta} := \left\{ \sum_{T \in \mathcal{T}_h} \vartheta_T^2 \right\}^{1/2}. \tag{4.3}$$

The following theorems constitute the main results of this section.

Theorem 4.1. *Assume that $\boldsymbol{f}$ is piecewise polynomial, and let $\vec{\boldsymbol{u}} := (\boldsymbol{u}, \omega, p) \in \mathbb{H}$ and $\vec{\boldsymbol{u}}_h := (\boldsymbol{u}_h, \omega_h, p_h) \in \mathbb{H}_h$ be the unique solutions of (2.4) and (3.2), respectively. Then, there exist constants $C_{\mathrm{rel}} > 0$ and $C_{\mathrm{eff}} > 0$, independent of h, such that*

$$C_{\mathrm{eff}}\, \boldsymbol{\theta} \leq \|\, \vec{\boldsymbol{u}} - \vec{\boldsymbol{u}}_h\,\|_{\mathbb{H}} \leq C_{\mathrm{rel}}\, \boldsymbol{\theta}\,. \tag{4.4}$$

Theorem 4.2. *Assume that $\boldsymbol{f}$ is piecewise polynomial, and let $\vec{\boldsymbol{u}} := (\boldsymbol{u}, \omega, p) \in \mathbb{H}$ and $\vec{\boldsymbol{u}}_h := (\boldsymbol{u}_h, \omega_h, p_h) \in \mathbb{H}_h$ be the unique solutions of (2.4) and (3.2), respectively. Then, there exist constants $c_{\mathrm{rel}} > 0$ and $c_{\mathrm{eff}} > 0$, independent of h, such that*

$$c_{\mathrm{eff}}\, \boldsymbol{\vartheta} \leq \|\, \vec{\boldsymbol{u}} - \vec{\boldsymbol{u}}_h\,\|_{\mathbb{H}} \leq c_{\mathrm{rel}}\, \boldsymbol{\vartheta}\,. \tag{4.5}$$

We remark that when $\boldsymbol{f}$ is not piecewise polynomial, then high order terms arising from suitable polynomial approximations of this function will appear in (4.4) and (4.5). The upper and lower bounds in these inequalities are known as the reliability and efficiency estimates, respectively, and they are

derived below in Sections 4.2 and 4.3. For this purpose, we will employ the Clément interpolation operator I_h, which maps $\mathrm{H}^1(\Omega)$ onto X_h (cf. [16]), where

$$X_h := \left\{ \varphi_h \in C(\bar{\Omega}) : \quad \varphi_h|_T \in P_1(T) \quad \forall\, T \in \mathcal{T}_h \right\}.$$

In addition, the local approximation properties of I_h are summarized as follows.

Lemma 4.3. *There exist c_1, $c_2 > 0$, independent of h, such that for all $\varphi \in \mathrm{H}^1(\Omega)$ there holds*

$$\|\varphi - I_h(\varphi)\|_{0,T} \leq c_1\, h_T\, \|\varphi\|_{1,\Delta(T)} \qquad \forall\, T \in \mathcal{T}_h$$

and

$$\|\varphi - I_h(\varphi)\|_{0,e} \leq c_2\, h_e^{1/2}\, \|\varphi\|_{1,\Delta(e)} \qquad \forall\, e \in \mathcal{E}_h(\Omega) \cup \mathcal{E}_h(\Gamma)\,,$$

where $\Delta(T) := \cup\{T' \in \mathcal{T}_h : \quad T' \cap T \neq \emptyset\}$ and $\Delta(e) := \cup\{T' \in \mathcal{T}_h : \quad T' \cap e \neq \emptyset\}$.

Proof. See [16]. □

4.2 Reliability of the a posteriori error estimators

We first deduce from the $\mathbb{H}$-ellipticity of $\mathcal{A}$ (cf. Lemma (2.2)) that there holds the global inf-sup condition

$$\alpha\, \|\vec{\boldsymbol{w}}\|_{\mathbb{H}} \leq \sup_{\substack{\vec{\boldsymbol{v}} \in \mathbb{H} \\ \vec{\boldsymbol{v}} \neq 0}} \frac{\mathcal{A}\,(\vec{\boldsymbol{w}},\, \vec{\boldsymbol{v}})}{\|\vec{\boldsymbol{v}}\|_{\mathbb{H}}} \qquad \forall\, \vec{\boldsymbol{w}} := (\boldsymbol{w}, \chi, r) \in \mathbb{H}\,. \tag{4.6}$$

Hence, we have the following preliminary estimate for the error.

Lemma 4.4. *Let $\vec{\boldsymbol{u}} := (\boldsymbol{u}, \omega, p) \in \mathbb{H}$ and $\vec{\boldsymbol{u}}_h := (\boldsymbol{u}_h, \omega_h, p_h) \in \mathbb{H}_h$ be the unique solutions of (2.4) and (3.2), respectively. Then, there exists a constant $c > 0$, independent of h, such that*

$$\|\vec{\boldsymbol{u}} - \vec{\boldsymbol{u}}_h\|_{\mathbb{H}} \leq C\, \|\, E\, \|_{\mathbb{H}'}\,,$$

where

$$E(\vec{\boldsymbol{v}}) := E_1(\boldsymbol{v}) + E_2(\eta) + E_3(q) \qquad \forall\, \vec{\boldsymbol{v}} := (\boldsymbol{v}, \eta, q\,) \in \mathbb{H}\,,$$

and $E_1 : \mathbf{H}_\Gamma\,(\mathrm{div};\, \Omega) \to \mathbb{R}$, $E_2 : \mathrm{H}^1_\Gamma(\Omega) \to \mathbb{R}$, and $E_3 : \mathrm{H}^1_\Sigma(\Omega) \to \mathbb{R}$ are the linear and bounded functionals defined by

$$E_1(\boldsymbol{v}) := \int_\Omega \mathbf{r}(\boldsymbol{u}_h, \omega_h) \cdot \boldsymbol{v} + \int_\Omega p_h\, \mathrm{div}\, \boldsymbol{v} - k_3 \int_\Omega \mathrm{div}\, \boldsymbol{u}_h\, \mathrm{div}\, \boldsymbol{v} \quad \forall\, \boldsymbol{v} \in \mathbf{H}_\Gamma(\mathrm{div};\, \Omega)\,, \tag{4.7}$$

$$E_2(\eta) := \nu\, \langle\, \boldsymbol{a} \cdot \boldsymbol{t},\, \eta \rangle_\Sigma - \nu \int_\Omega \omega_h\, \eta + \nu \int_\Omega \boldsymbol{u}_h \cdot \mathbf{curl}\, \eta + k_1 \int_\Omega \mathbf{r}(\boldsymbol{u}_h, \omega_h) \cdot \mathbf{curl}\, \eta \quad \forall\, \eta \in \mathrm{H}^1_\Gamma(\Omega)\,, \tag{4.8}$$

and

$$E_3(q) := k_2 \int_\Omega \mathbf{r}(\boldsymbol{u}_h, p_h) \cdot \nabla\, q \quad - \int_\Omega q\, \mathrm{div}\, \boldsymbol{u}_h \qquad \forall\, q \in \mathrm{H}^1_\Sigma(\Omega)\,. \tag{4.9}$$

In addition, there holds

$$E(\vec{\boldsymbol{v}}_h) = 0 \qquad \forall\, \vec{\boldsymbol{v}}_h := (\boldsymbol{v}_h, \eta_h, q_h) \in \mathbb{H}_h\,. \tag{4.10}$$

Proof. Applying (4.6) to the error $\vec{\boldsymbol{w}} := \vec{\boldsymbol{u}} - \vec{\boldsymbol{u}}_h$, and then employing (2.4) and the definitions of $\mathcal{A}$ and $\mathcal{G}$ (cf. (2.5) and (2.6)), we arrive at

$$\alpha \, \|\vec{\boldsymbol{u}} - \vec{\boldsymbol{u}}_h\|_{\mathbb{H}} \leq \sup_{\substack{\vec{\boldsymbol{v}} \in \mathbb{H} \\ \vec{\boldsymbol{v}} \neq 0}} \frac{\mathcal{G}(\vec{\boldsymbol{v}}) - \mathcal{A}(\vec{\boldsymbol{u}}_h, \vec{\boldsymbol{v}})}{\|\vec{\boldsymbol{v}}\|_{\mathbb{H}}} := \|\mathcal{G} - \mathcal{A}(\vec{\boldsymbol{u}}_h, \cdot)\|_{\mathbb{H}'} ,$$

where, bearing in mind (4.7), (4.8), and (4.9), there holds

$$\mathcal{G}(\vec{\boldsymbol{v}}) - \mathcal{A}(\vec{\boldsymbol{u}}_h, \vec{\boldsymbol{v}}) = E_1(\boldsymbol{v}) + E_2(\eta) + E_3(q) \qquad \forall \, \vec{\boldsymbol{v}} := (\boldsymbol{v}, \eta, q) \in \mathbb{H} .$$

Moreover, it is straightforward from (3.2) that $\mathcal{G}(\vec{\boldsymbol{v}}_h) - \mathcal{A}(\vec{\boldsymbol{u}}_h, \vec{\boldsymbol{v}}_h) = 0 \quad \forall \, \vec{\boldsymbol{v}}_h := (\boldsymbol{v}_h, \eta_h, q_h) \in \mathbb{H}_h$, which, denoting $E := \mathcal{G} - \mathcal{A}(\vec{\boldsymbol{u}}_h, \cdot)$, gives (4.10) and ends the proof. □

In order to complete the derivation of the a posteriori error estimates, we need to obtain a suitable upper bound for $\|E\|_{\mathbb{H}'}$. This is done independently for $\boldsymbol{\theta}$ and $\boldsymbol{\vartheta}$ in the subsequent sections.

4.2.1 Reliability of $\boldsymbol{\theta}$

We use once the Clément interpolation operator I_h. More precisely, given $\vec{\boldsymbol{v}} := (\boldsymbol{v}, \eta, q) \in \mathbb{H}$, we let

$$\vec{\boldsymbol{v}_h} := (\boldsymbol{0}, I_h(\eta), 0) \in \mathbb{H}_h ,$$

so that, using (4.10), we find that

$$E(\vec{\boldsymbol{v}}) = E_1(\boldsymbol{v}) + E_2(\eta - I_h(\eta)) + E_3(q) . \tag{4.11}$$

Note here that the fact that I_h preserves Dirichlet boundary conditions (cf. [16]) ensures that $I_h(\eta)$ also vanishes on Γ.

Furthermore, it is easy to see that

$$E_2(\eta - I_h(\eta)) = E_{21}(\eta - I_h(\eta)) + E_{22}(\eta - I_h(\eta)) , \tag{4.12}$$

where

$$E_{21}(\eta - I_h(\eta)) := \nu \, \langle \boldsymbol{a} \cdot \boldsymbol{t}, \, \eta - \eta_h \rangle_{\Sigma} - \nu \int_{\Omega} \omega_h (\eta - \eta_h) + \nu \int_{\Omega} \boldsymbol{u}_h \cdot \mathbf{curl}(\eta - \eta_h) \tag{4.13}$$

and

$$E_{22}(\eta - I_h(\eta)) := k_1 \int_{\Omega} \mathbf{r}(\boldsymbol{u}_h, \omega_h) \cdot \mathbf{curl}(\eta - \eta_h) . \tag{4.14}$$

Consequently, in order to estimate $|E(\vec{\boldsymbol{v}})|$ in terms of residual terms and $\|\vec{\boldsymbol{v}}\|_{\mathbb{H}}$, thus deriving a suitable bound for $\|E\|_{\mathbb{H}'}$, we now proceed to get upper bounds for each one of the above components.

Lemma 4.5. *There exists $C > 0$, independent of h, such that*

$$|E_1(\boldsymbol{v})| + |E_3(q)| \leq C \left\{ \sum_{T \in \mathcal{T}_h} \widetilde{\theta}_T^2 \right\}^{1/2} \|\vec{\boldsymbol{v}}\|_{\mathbb{H}} \qquad \forall \, \vec{\boldsymbol{v}} := (\boldsymbol{v}, \eta, q) \in \mathbb{H} ,$$

where

$$\widetilde{\theta}_T^2 := \left\| \mathbf{r}(\boldsymbol{u}_h, \omega_h, p_h) \right\|_{0,T}^2 + \left\| \operatorname{div} \boldsymbol{u}_h \right\|_{0,T}^2 \qquad \forall \, T \in \mathcal{T}_h .$$

Proof. Let $\vec{\boldsymbol{v}} := (\boldsymbol{v}, \eta, q) \in \mathbb{H}$. Integrating by parts in Ω and using that $p_h = 0$ on Σ and that $\boldsymbol{v} \cdot \boldsymbol{n} = 0$ on Γ, we get

$$\int_\Omega p_h \operatorname{div} \boldsymbol{v} \;=\; -\int_\Omega \nabla\, p_h \cdot \boldsymbol{v}\,,$$

which, according to (4.7), yields

$$E_1(\boldsymbol{v}) \;=\; \int_\Omega \mathbf{r}(\boldsymbol{u}_h, \omega_h, p_h) \cdot \boldsymbol{v} \;-\; k_3 \int_\Omega \operatorname{div} \boldsymbol{u}_h \operatorname{div} \boldsymbol{v}\,. \tag{4.15}$$

In turn, integrating by parts again in Ω and using now that $\nabla q \cdot \boldsymbol{t} = 0$ on Σ (since q vanishes there), $\omega_h = 0$ on Γ, and certainly $\operatorname{rot} \nabla q = 0$, we find that

$$\int_\Omega \mathbf{curl}\, \omega_h \cdot \nabla q \;=\; 0\,,$$

which implies, together with (4.9), that

$$E_3(q) \;:=\; k_2 \int_\Omega \mathbf{r}(\boldsymbol{u}_h, \omega_h, p_h) \cdot \nabla q \quad\; - \int_\Omega q \operatorname{div} \boldsymbol{u}_h\,. \tag{4.16}$$

Hence, the proof follows from straightforward applications of the Cauchy-Schwarz inequality in (4.15) and (4.16). □

Lemma 4.6. *There exists $C > 0$, independent of h, such that*

$$|E_{21}(\eta - I_h(\eta))| \;\leq\; C \left\{ \sum_{T \in \mathcal{T}_h} \widehat{\theta}_T^2 \right\}^{1/2} \|\vec{\boldsymbol{v}}\|_{\mathbb{H}} \qquad \forall\, \vec{\boldsymbol{v}} := (\boldsymbol{v}, \eta, q) \;\in\; \mathbb{H}\,,$$

where

$$\widehat{\theta}_T^2 \;:=\; h_T^2 \,\|\operatorname{rot} \boldsymbol{u}_h - \omega_h\|_{0,T}^2 \;+ \sum_{e \in \mathcal{E}(T) \cap \mathcal{E}_h(\Omega)} h_e \,\|[\boldsymbol{u}_h \cdot \boldsymbol{t}]\|_{0,e}^2 \;+ \sum_{e \in \mathcal{E}(T) \cap \mathcal{E}_h(\Sigma)} h_e \,\|\boldsymbol{a} \cdot \boldsymbol{t} - \boldsymbol{u}_h \cdot \boldsymbol{t}\|_{0,e}^2\,.$$

Proof. We begin by looking at the third term defining E_{21} (cf. (4.13)). In fact, integrating by parts in each $T \in \mathcal{T}_h$, we obtain

$$\int_\Omega \boldsymbol{u}_h \cdot \mathbf{curl}(\eta - I_h(\eta)) \;=\; \sum_{T \in \mathcal{T}_h} \left\{ \int_T \operatorname{rot} \boldsymbol{u}_h \,(\eta - I_h(\eta)) \;- \int_{\partial T} \boldsymbol{u}_h \cdot \boldsymbol{t}\,(\eta - I_h(\eta)) \right\},$$

which, using that $\eta = I_h(\eta) = 0$ on Γ, yields

$$\begin{aligned} \int_\Omega \boldsymbol{u}_h \cdot \mathbf{curl}(\eta - I_h(\eta)) \;=\; & \sum_{T \in \mathcal{T}_h} \int_T \operatorname{rot} \boldsymbol{u}_h \,(\eta - I_h(\eta)) \;- \sum_{e \in \mathcal{E}_h(\Omega)} \int_e [\boldsymbol{u}_h \cdot \boldsymbol{t}]\,(\eta - I_h(\eta)) \\ & - \sum_{e \in \mathcal{E}_h(\Sigma)} \int_e \boldsymbol{u}_h \cdot \boldsymbol{t}\,(\eta - I_h(\eta))\,. \end{aligned}$$

It follows from (4.13) and the foregoing equality that

$$\begin{aligned} E_{21}(\eta - I_h(\eta)) \;=\; & \nu \sum_{T \in \mathcal{T}_h} \int_T \Big\{ \operatorname{rot} \boldsymbol{u}_h - \omega_h \Big\}\,(\eta - I_h(\eta)) \;- \nu \sum_{e \in \mathcal{E}_h(\Omega)} \int_e [\boldsymbol{u}_h \cdot \boldsymbol{t}]\,(\eta - I_h(\eta)) \\ & + \;\; \nu \sum_{e \in \mathcal{E}_h(\Sigma)} \int_e \Big\{ \boldsymbol{a} \cdot \boldsymbol{t} - \boldsymbol{u}_h \cdot \boldsymbol{t} \Big\}\,(\eta - I_h(\eta))\,, \end{aligned}$$

and hence the proof is completed by applying Cauchy-Schwarz inequality, the approximation properties of the Clément interpolant I_h (cf. Lemma 4.3), and the fact that the number of triangles of $\Delta(T)$ and $\Delta(e)$ are bounded independently of $T \in \mathcal{T}_h$ and $e \in \mathcal{E}_h$, respectively. □

Lemma 4.7. *There exists $C > 0$, independent of h, such that*

$$|E_{22}(\eta - I_h(\eta))| \,\leq\, C \left\{ \sum_{T \in \mathcal{T}_h} \overline{\theta}_T^2 \right\}^{1/2} \|\vec{\boldsymbol{v}}\|_{\mathbb{H}} \qquad \forall\, \vec{\boldsymbol{v}} := (\boldsymbol{v}, \eta, q) \,\in\, \mathbb{H}\,,$$

where

$$\overline{\theta}_T^2 := h_T^2 \left\| \operatorname{rot} \left\{ \mathbf{r}(\boldsymbol{u}_h, \omega_h) \right\} \right\|_{0,T}^2 + \sum_{e \in \mathcal{E}(T) \cap \mathcal{E}_h(\Omega)} h_e \left\| \left[\mathbf{r}(\boldsymbol{u}_h, \omega_h) \cdot \boldsymbol{t} \right] \right\|_{0,e}^2 + \sum_{e \in \mathcal{E}(T) \cap \mathcal{E}_h(\Sigma)} h_e \left\| \mathbf{r}(\boldsymbol{u}_h, \omega_h) \cdot \boldsymbol{t} \right\|_{0,e}^2 .$$

Proof. It follows from (4.14), integrating by parts in each $T \in \mathcal{T}_h$, that

$$E_{22}(\eta \,-\, I_h(\eta)) \,=\, k_1 \sum_{T \in \mathcal{T}_h} \left\{ \int_T (\eta - I_h(\eta)) \, \operatorname{rot} \left\{ \mathbf{r}(\boldsymbol{u}_h, \omega_h) \right\} \,-\, \int_{\partial T} (\eta - I_h(\eta)) \, \mathbf{r}(\boldsymbol{u}_h, \omega_h) \cdot \boldsymbol{t} \right\},$$

which, using that $\eta = I_h(\eta) = 0$ on Γ, yields

$$\begin{aligned} E_{22}(\eta \,-\, I_h(\eta)) \,&=\, k_1 \sum_{T \in \mathcal{T}_h} \int_T (\eta - I_h(\eta)) \, \operatorname{rot} \left\{ \mathbf{r}(\boldsymbol{u}_h, \omega_h) \right\} \\ -\quad k_1 \sum_{e \in \mathcal{E}_h(\Omega)} \int_e (\eta - I_h(\eta)) \left[\mathbf{r}(\boldsymbol{u}_h, \omega_h) \cdot \boldsymbol{t} \right] \,&-\, k_1 \sum_{e \in \mathcal{E}_h(\Sigma)} \int_e (\eta - I_h(\eta)) \, \mathbf{r}(\boldsymbol{u}_h, \omega_h) \cdot \boldsymbol{t} \,. \end{aligned}$$

In this way, proceeding as in the previous proof, that is applying Cauchy-Schwarz inequality, the approximation properties of I_h, and the uniform boundedness of the number of triangles of $\Delta(T)$ and $\Delta(e)$, the proof is concluded. □

We end this section by remarking that the reliability estimate for $\boldsymbol{\theta}$ (cf. upper estimate in (4.4), Theorem 4.1) follows from identities (4.11), (4.12), (4.13), and (4.14), together with Lemmata 4.4, 4.5, 4.6, and 4.7.

4.2.2 Reliability of ϑ

In what follows we bound $\|E\|_{\mathbb{H}'}$ (cf. Lemma 4.4) by using twice the Clément interpolant I_h. More precisely, given $\vec{\boldsymbol{v}} := (\boldsymbol{v}, \eta, q) \in \mathbb{H}$, we now let

$$\vec{\boldsymbol{v}_h} \,:=\, (0, I_h(\eta), I_h(q)) \,\in\, \mathbb{H}_h \,,$$

so that, using (4.10), we find that

$$E(\vec{\boldsymbol{v}}) \,=\, E_1(\boldsymbol{v}) \,+\, E_2(\eta \,-\, I_h(\eta)) \,+\, E_3(q - I_h(q)) \,, \tag{4.17}$$

where $E_1(\boldsymbol{v})$ and $E_2(\eta \,-\, I_h(\eta))$ are given by (4.7) and (4.12) - (4.14), respectively, and

$$E_3(q - I_h(q)) \,:=\, k_2 \int_\Omega \mathbf{r}(\boldsymbol{u}_h, p_h) \cdot \nabla \, (q - I_h(q)) \quad - \int_\Omega (q - I_h(q)) \operatorname{div} \boldsymbol{u}_h \,. \tag{4.18}$$

Note here that the fact that I_h preserves Dirichlet boundary conditions (cf. [16]) ensures now that $I_h(\eta)$ and $I_h(q)$ also vanish on Γ and Σ, respectively.

Similarly as in Section 4.2.1, in order to estimate $|E(\vec{\boldsymbol{v}})|$ in terms of residual terms and $\|\vec{\boldsymbol{v}}\|_{\mathbb{H}}$, thus deriving an alternative bound for $\|E\|_{\mathbb{H}'}$, we now proceed to get upper bounds for each one of the components in (4.17). Actually, since the estimates for $E_1(\boldsymbol{v})$ and $E_2(\eta - I_h(\eta))$ are already available from Lemma 4.5, (4.12) and Lemmata 4.6 and 4.7, we just concentrate on the remaining third term.

Lemma 4.8. *There exists $C > 0$, independent of h, such that*

$$|E_3(q - I_h(q))| \,\leq\, C \left\{ \sum_{T \in \mathcal{T}_h} \overline{\vartheta}_T^2 \right\}^{1/2} \|\vec{\boldsymbol{v}}\|_{\mathbb{H}} \qquad \forall\, \vec{\boldsymbol{v}} := (\boldsymbol{v}, \eta, q) \,\in\, \mathbb{H}\,,$$

where

$$\begin{aligned} \overline{\vartheta}_T^2 \,:=\, & h_T^2 \left\| \mathrm{div}\big\{ \mathbf{r}(\boldsymbol{u}_h, p_h) \big\} \right\|_{0,T}^2 \,+\, h_T^2 \, \|\mathrm{div}\, \boldsymbol{u}_h\|_{0,T}^2 \\ & + \sum_{e \in \mathcal{E}(T) \cap \mathcal{E}_h(\Omega)} h_e \left\| \big[\mathbf{r}(\boldsymbol{u}_h, p_h) \cdot \boldsymbol{n} \big] \right\|_{0,e}^2 + \sum_{e \in \mathcal{E}(T) \cap \mathcal{E}_h(\Gamma)} h_e \left\| \mathbf{r}(\boldsymbol{u}_h, p_h) \cdot \boldsymbol{n} \right\|_{0,e}^2 . \end{aligned}$$

Proof. It is very similar to the proof of Lemma 4.7. Indeed, it follows from (4.18), integrating by parts in each $T \in \mathcal{T}_h$, that

$$\begin{aligned} E_3(q \,-\, I_h(q)) \,=\, -\, k_2 \sum_{T \in \mathcal{T}_h} & \left\{ \int_T (q - I_h(q)) \, \mathrm{div}\big\{ \mathbf{r}(\boldsymbol{u}_h, p_h) \big\} \,-\, \int_{\partial T} (q - I_h(q)) \, \mathbf{r}(\boldsymbol{u}_h, p_h) \cdot \boldsymbol{n} \right\} \\ & - \quad \int_\Omega (q - I_h(q)) \, \mathrm{div}\, \boldsymbol{u}_h \,, \end{aligned}$$

which, using that $q = I_h(q) = 0$ on Σ, yields

$$\begin{aligned} E_3(q - I_h(q)) \,=\, & -\, k_2 \sum_{T \in \mathcal{T}_h} \int_T (q - I_h(q)) \, \mathrm{div}\big\{ \mathbf{r}(\boldsymbol{u}_h, p_h) \big\} \,-\, \sum_{T \in \mathcal{T}_h} \int_T (q - I_h(q)) \, \mathrm{div}\, \boldsymbol{u}_h \\ + \quad & \kappa_2 \sum_{e \in \mathcal{E}_h(\Omega)} \int_e (q - I_h(q)) \, \big[\mathbf{r}(\boldsymbol{u}_h, p_h) \cdot \boldsymbol{n} \big] \,+\, k_2 \sum_{e \in \mathcal{E}_h(\Gamma)} \int_e (q - I_h(q)) \, \mathbf{r}(\boldsymbol{u}_h, p_h) \cdot \boldsymbol{n} \,. \end{aligned}$$

In this way, proceeding as in previous proofs of this section, the required inequality is obtained by applying Cauchy-Schwarz inequality, the approximation properties of I_h, and the uniform boundedness of the number of triangles of $\Delta(T)$ and $\Delta(e)$. □

Hence, according to (4.17), the reliability of $\boldsymbol{\vartheta}$ (cf. upper bound in (4.5)) is consequence of Lemma 4.8, and the estimate for $E_1(\boldsymbol{v})$ and $E_2(\eta - I_h(\eta))$ provided by Lemmata 4.5, 4.6 and 4.7 in Section 4.2.1.

4.3 Efficiency of the a posteriori error estimators

In this section we show the efficiency of our a posteriori error estimators $\boldsymbol{\theta}$ (cf. (4.1)) and $\boldsymbol{\vartheta}$ (cf. (4.2)). Equivalently, we provide upper bounds depending on the actual errors for the eight terms defining the local indicator θ_T^2 and for the remaining three terms that complete the definition of $\boldsymbol{\vartheta}$. The easiest

ones are the first two terms defining $\boldsymbol{\theta}$, for which, using from Theorem 2.1 that $\boldsymbol{f} = \sigma\boldsymbol{u} + \nu\,\mathbf{curl}\,\omega + \nabla p$ and $\mathrm{div}\,\boldsymbol{u} = 0$ in Ω, we find that

$$\begin{aligned}\|\mathbf{r}(\boldsymbol{u}_h,\omega_h,p_h)\|_{0,T}^2 \;&=\; \big\|\{\sigma\,\boldsymbol{u} \,+\, \nu\;\mathbf{curl}\,\omega \,+\, \nabla p\} \,-\, \sigma\,\boldsymbol{u}_h \,-\, \nu\;\mathbf{curl}\,\omega_h \,-\, \nabla p_h\big\|_{0,T}^2 \\ &\leq\; C\left\{\|\boldsymbol{u}-\boldsymbol{u}_h\|_{0,T}^2 \,+\, |\omega-\omega_h|_{1,T}^2 \,+\, |p-p_h|_{1,T}^2\right\},\end{aligned} \tag{4.19}$$

where $C := \sigma^2 + \nu^2 + 1$, and

$$\|\mathrm{div}\,\boldsymbol{u}_h\|_{0,T}^2 \;=\; \|\mathrm{div}\,(\boldsymbol{u}_h - \boldsymbol{u})\|_{0,T}^2 \;\leq\; \|\boldsymbol{u}-\boldsymbol{u}_h\|_{\mathrm{div},\Omega}^2\,. \tag{4.20}$$

The derivation of the corresponding upper bounds for the remaining terms in (4.1) and (4.2) is performed next. To this end, we proceed as in [13] and [27], and apply the localization technique based on triangle-bubble and edge-bubble functions, together with extension operators and inverse inequalities. Therefore, we now introduce further notations and preliminary results. Given $T \in \mathcal{T}_h$ and $e \in \mathcal{E}(T)$, we let ψ_T and ψ_e be the usual triangle-bubble and edge-bubble functions, respectively (see [44, eqs. (1.5) and (1.6)]), which satisfy:

ii) $\psi_T \in P_3(T)$, $\psi_T = 0$ on ∂T, $\mathrm{supp}(\psi_T) \subseteq T$, and $0 \leq \psi_T \leq 1$ in T.

ii) $\psi_e|_T \in P_2(T)$, $\psi_e = 0$ on $\partial T \setminus e$, $\mathrm{supp}(\psi_e) \subseteq w_e := \cup\{T' \in \mathcal{T}_h :\; e \in \mathcal{E}(T')\}$, and $0 \leq \psi_e \leq 1$ in w_e.

We also know from [43] that, given $k \in \mathbb{N}\cup\{0\}$, there exists an extension operator $L : C(e) \to C(T)$ that satisfies $L(p) \in P_k(T)$ and $L(p)|_e = p$ for all $p \in P_k(e)$. Additional properties of ψ_T, ψ_e and L are collected in the following lemma.

Lemma 4.9. *Given $k \in \mathbb{N}\cup\{0\}$, there exist positive constants c_1, c_2, and c_3, depending only on k and the shape regularity of the triangulations (minimum angle condition), such that for each $T \in \mathcal{T}_h$ and $e \in \mathcal{E}(T)$, there hold*

$$\|q\|_{0,T}^2 \leq c_1\|\psi_T^{1/2}q\|_{0,T}^2 \qquad \forall q \in P_k(T) \tag{4.21}$$

$$\|p\|_{0,e}^2 \leq c_2\|\psi_e^{1/2}p\|_{0,e}^2 \qquad \forall p \in P_k(e) \tag{4.22}$$

and

$$\|\psi_e^{1/2}L(p)\|_{0,T}^2 \leq c_3\,h_e\|p\|_{0,e}^2 \qquad \forall p \in P_k(e) \tag{4.23}$$

Proof. See [43, Lemma 4.1]. □

The following inverse inequality is also employed.

Lemma 4.10. *Let k, l, $m \in \mathbb{N}\cup\{0\}$ such that $l \leq m$. Then there exists $c > 0$, depending only on k, l, m and the shape regularity of the triangulations, such that for each $T \in \mathcal{T}_h$ there holds*

$$|q|_{m,T} \;\leq\; c\,h_T^{l-m}\,|q|_{l,T} \qquad \forall\, q \in P_k(T)\,. \tag{4.24}$$

Proof. See [15, Theorem 3.2.6]. □

We continue our efficiency analysis with the estimate for the third term defining (4.1).

Lemma 4.11. *There exists $C > 0$, independent of h, such that*

$$h_T^2 \, \| \operatorname{rot} \boldsymbol{u}_h \, - \, \omega_h \, \|_{0,T}^2 \, \leq \, C \left\{ \|\boldsymbol{u} - \boldsymbol{u}_h\|_{0,T}^2 \, + \, h_T^2 \, \|\omega - \omega_h\|_{0,T}^2 \right\} \qquad \forall \, T \in \mathcal{T}_h \, . \tag{4.25}$$

Proof. It is similar to the proof of [27, Lemma 20]. Given $T \in \mathcal{T}_h$ we denote $\gamma_T := \operatorname{rot} \boldsymbol{u}_h \, - \, \omega_h$ in T. Applying (4.21) to γ_T and then using from Theorem 2.1 that $\operatorname{rot} \boldsymbol{u} = \omega$ in Ω, we find that

$$\begin{aligned} \|\gamma_T\|_{0,T}^2 \, &\leq \, c_1 \, \|\psi_T^{1/2} \gamma_T\|_{0,T}^2 \, = \, c_1 \int_T \psi_T \, \gamma_T \left\{ \operatorname{rot} \boldsymbol{u}_h \, - \, \omega_h \right\} \\ &= \, - \, c_1 \int_T \psi_T \, \gamma_T \operatorname{rot}(\boldsymbol{u} - \boldsymbol{u}_h) \, + \, c_1 \int_T \psi_T \, \gamma_T \, (\omega - \omega_h) \, . \end{aligned} \tag{4.26}$$

Next, integrating by parts in T and recalling that ψ_T vanishes on ∂T, we obtain

$$\int_T \psi_T \, \gamma_T \operatorname{rot}(\boldsymbol{u} - \boldsymbol{u}_h) \, = \, \int_T (\boldsymbol{u} - \boldsymbol{u}_h) \cdot \mathbf{curl}(\psi_T \, \gamma_T) \, ,$$

which replaced back into (4.26) leads to

$$\|\gamma_T\|_{0,T}^2 \, \leq \, - \, c_1 \int_T (\boldsymbol{u} - \boldsymbol{u}_h) \cdot \mathbf{curl}(\psi_T \, \gamma_T) \, + \, c_1 \int_T \psi_T \, \gamma_T \, (\omega - \omega_h) \, . \tag{4.27}$$

Hence, applying the Cauchy-Schwarz inequality and the inverse estimate (4.24), we easily deduce from (4.27) that

$$\|\gamma_T\|_{0,T}^2 \, \leq \, C \, \|\psi_T \, \gamma_T\|_{0,T} \left\{ h_T^{-1} \, \|\boldsymbol{u} - \boldsymbol{u}_h\|_{0,T} \, + \, \|\omega - \omega_h\|_{0,T} \right\} ,$$

which yields

$$h_T \, \|\gamma_T\|_{0,T} \, \leq \, C \left\{ \|\boldsymbol{u} - \boldsymbol{u}_h\|_{0,T} \, + \, h_T \, \|\omega - \omega_h\|_{0,T} \right\} ,$$

thus implying (4.25) and completing the proof. □

We now aim to estimate the terms involving $\mathbf{r}(\boldsymbol{u}_h, \omega_h)$. The following lemma, whose proof makes use of Lemmas 4.9 and 4.10, will be employed for this purpose.

Lemma 4.12. *Let $\boldsymbol{\rho}_h \in \mathbf{L}^2(\Omega)$ be a piecewise polynomial of degree $k \geq 0$ on each $T \in \mathcal{T}_h$, and let $\boldsymbol{\rho} \in \mathbf{L}^2(\Omega)$ be such that $\operatorname{rot} \{\boldsymbol{\rho}\} = 0$ in Ω. Then, there exist $c, \widetilde{c} > 0$, independent of h, such that*

$$h_T^2 \, \| \operatorname{rot} \{\boldsymbol{\rho}_h\} \|_{0,T}^2 \, \leq \, c \, \|\boldsymbol{\rho} - \boldsymbol{\rho}_h\|_{0,T}^2 \qquad \forall \, T \in \mathcal{T}_h \, , \tag{4.28}$$

and

$$h_e \, \|[\boldsymbol{\rho}_h \cdot \boldsymbol{t}]\|_{0,e}^2 \, \leq \, \widetilde{c} \, \|\boldsymbol{\rho} - \boldsymbol{\rho}_h\|_{0,w_e}^2 \qquad \forall \, e \in \mathcal{E}_h(\Omega) \, . \tag{4.29}$$

Proof. For the proof of (4.28) we refer to [6, Lemma 4.3], whereas (4.29) is a slight modification of the proof of [6, Lemma 4.4]. We omit further details. □

As a straightforward consequence of the foregoing lemma we have the following result.

Lemma 4.13. *There exist C_1, $C_2 > 0$, independent of h, such that*

$$h_T^2 \, \| \operatorname{rot} \{\mathbf{r}(\boldsymbol{u}_h, \omega_h)\} \|_{0,T}^2 \, \leq \, C_1 \left\{ \|\boldsymbol{u} - \boldsymbol{u}_h\|_{0,T}^2 \, + \, |\omega - \omega_h|_{1,T}^2 \right\} \qquad \forall \, T \in \mathcal{T}_h \, , \tag{4.30}$$

and

$$h_e \, \| [\mathbf{r}(\boldsymbol{u}_h, \omega_h) \cdot \boldsymbol{t}] \, \|_{0,e}^2 \, \leq \, C_2 \left\{ \|\boldsymbol{u} - \boldsymbol{u}_h\|_{0,w_e}^2 \, + \, |\omega - \omega_h|_{1,w_e}^2 \right\} \qquad \forall \, e \in \mathcal{E}_h(\Omega) \, . \tag{4.31}$$

Proof. Since $\operatorname{rot} \nabla p = 0$ in Ω and, according to Theorem 2.1, $\nabla p = \boldsymbol{f} - \sigma \boldsymbol{u} - \nu \, \mathbf{curl} \, \omega$ in Ω, it suffices to apply Lemma 4.12 to $\boldsymbol{\rho} = \nabla p$ and $\boldsymbol{\rho}_h = \mathbf{r}(\boldsymbol{u}_h, \omega_h)$, and then employ the triangle inequality. □

The third term involving $\mathbf{r}(\boldsymbol{u}_h, \omega_h)$ is estimated next.

Lemma 4.14. *There exists $C > 0$, independent of h, such that*

$$h_e \, \|\mathbf{r}(\boldsymbol{u}_h, \omega_h) \cdot \boldsymbol{t}\|_{0,e}^2 \, \leq \, C \left\{ \|\boldsymbol{u} - \boldsymbol{u}_h\|_{0,T_e}^2 \, + \, |\omega - \omega_h|_{1,T_e}^2 \right\} \qquad \forall \, e \in \mathcal{E}_h(\Sigma) \, , \tag{4.32}$$

where T_e is the triangle of $\mathcal{T}_h$ having e as an edge.

Proof. It follows as in the proof of [27, Lemma 21] (see also [32, Lemma 5.17]). In fact, given $e \in \mathcal{E}_h(\Sigma)$ we set $\gamma_e := \mathbf{r}(\boldsymbol{u}_h, \omega_h) \cdot \boldsymbol{t}$ on e. Since $p = 0$ on Σ (cf. Theorem 2.1), there holds $\nabla p \cdot \boldsymbol{t} = 0$ on Σ, and hence

$$\mathbf{r}(\boldsymbol{u}_h, \omega_h) \cdot \boldsymbol{t} = \left\{ \mathbf{r}(\boldsymbol{u}_h, \omega_h) - \nabla p \right\} \cdot \boldsymbol{t} \quad \text{on} \quad e \, .$$

Then, applying (4.22) and the extension operator $L : C(e) \to C(T)$, we obtain that

$$\begin{aligned} \|\gamma_e\|_{0,e}^2 \, &\leq \, c_2 \, \|\psi_e^{1/2} \, \gamma_e\|_{0,e}^2 \, = \, c_2 \int_e \psi_e \, \gamma_e \left\{ \mathbf{r}(\boldsymbol{u}_h, \omega_h) \cdot \boldsymbol{t} \right\} \\ &= \quad c_2 \int_{\partial T_e} \psi_e \, L(\gamma_e) \left\{ \left\{ \mathbf{r}(\boldsymbol{u}_h, \omega_h) - \nabla p \right\} \cdot \boldsymbol{t} \right\} . \end{aligned} \tag{4.33}$$

Now, integrating by parts and using that $\operatorname{rot} \left\{ \nabla p \right\} \, = \, 0$ in Ω, we find that

$$\begin{aligned} &\int_{\partial T_e} \psi_e \, L(\gamma_e) \left\{ \left\{ \mathbf{r}(\boldsymbol{u}_h, \omega_h) - \nabla p \right\} \cdot \boldsymbol{t} \right\} \\ &= \quad - \int_{T_e} \mathbf{curl}(\psi_e \, L(\gamma_e)) \cdot \left\{ \mathbf{r}(\boldsymbol{u}_h, \omega_h) - \nabla p \right\} \, + \, \int_{T_e} \psi_e \, L(\gamma_e) \, \operatorname{rot} \left\{ \mathbf{r}(\boldsymbol{u}_h, \omega_h) \right\} . \end{aligned} \tag{4.34}$$

In turn, thanks to the fact that $0 \, \leq \, \psi_e \, \leq \, 1$ and (4.23), we have that

$$\|\psi_e \, L(\gamma_e)\|_{0,T_e} \, \leq \, \|\psi_e^{1/2} \, L(\gamma_e)\|_{0,T_e} \, \leq \, c \, h_e^{1/2} \|\gamma_e\|_{0,e} \, . \tag{4.35}$$

Hence, applying the Cauchy-Schwarz inequality and the inverse estimate (4.24), and recalling from Theorem 2.1 that $\nabla p = \boldsymbol{f} - \sigma \boldsymbol{u} - \nu \, \mathbf{curl} \, \omega$ in Ω, we deduce from (4.33), (4.34), and (4.35) that

$$\|\gamma_e\|_{0,e}^2 \, \leq \, C \left\{ h_{T_e}^{-1} \left\{ \|\boldsymbol{u} - \boldsymbol{u}_h\|_{0,T_e} + |\omega - \omega_h|_{1,T_e} \right\} \, + \, \| \operatorname{rot} \left\{ \mathbf{r}(\boldsymbol{u}_h, \omega_h) \right\} \|_{0,T_e} \right\} \, h_e^{1/2} \, \|\gamma_e\|_{0,e} \, ,$$

which, using that $h_e \leq h_{T_e}$, yields

$$h_e \, \|\gamma_e\|_{0,e}^2 \, \leq \, C \left\{ \|\boldsymbol{u} - \boldsymbol{u}_h\|_{0,T_e}^2 \, + \, |\omega - \omega_h|_{1,T_e}^2 \, + \, h_{T_e}^2 \, \| \operatorname{rot} \left\{ \mathbf{r}(\boldsymbol{u}_h, \omega_h) \right\} \|_{0,T_e}^2 \right\} .$$

This inequality and the upper bound for $h_{T_e}^2 \, \| \operatorname{rot} \left\{ \mathbf{r}(\boldsymbol{u}_h, \omega_h) \right\} \|_{0,T_e}^2$ (cf. (4.30)) imply (4.32) and complete the proof. □

We continue our efficiency analysis with the estimates involving $\boldsymbol{u}_h \cdot \boldsymbol{t}$, which are provided in the following two lemmata.

Lemma 4.15. *There exists $C > 0$, independent of h, such that*

$$h_e \, \|[\boldsymbol{u}_h \cdot \boldsymbol{t}]\|_{0,e}^2 \, \leq \, C \sum_{T \subseteq w_e} \Big\{ \|\boldsymbol{u} - \boldsymbol{u}_h\|_{0,T}^2 \, + \, h_T^2 \, \|\omega - \omega_h\|_{0,T}^2 \Big\} \qquad \forall \, e \in \mathcal{E}_h(\Omega) \, . \tag{4.36}$$

Proof. Given $e \in \mathcal{E}_h(\Omega)$, we set $\gamma_e := [\boldsymbol{u}_h \cdot \boldsymbol{t}]$ on e. Hence, applying (4.22), and then employing the extension operator $L : C(e) \to C(T)$ together with the integration by parts formula on each $T \subseteq w_e$, we obtain that

$$\begin{aligned} \|\gamma_e\|_{0,e}^2 \, &\leq \, c_2 \, \|\psi_e^{1/2} \, \gamma_e\|_{0,e}^2 \, = \, c_2 \int_e \psi_e \, L(\gamma_e) \, [\boldsymbol{u}_h \cdot \boldsymbol{t}] \\ &= \, c_2 \left\{ \int_{w_e} \mathrm{rot} \, \boldsymbol{u}_h \, \psi_e \, L(\gamma_e) \, - \, \int_{w_e} \boldsymbol{u}_h \cdot \mathbf{curl} \left\{ \psi_e \, L(\gamma_e) \right\} \right\} , \end{aligned} \tag{4.37}$$

where, after adding and substracting both ω_h and ω, we can write

$$\int_{w_e} \mathrm{rot} \, \boldsymbol{u}_h \, \psi_e \, L(\gamma_e) \, = \, \int_{w_e} \big\{ \mathrm{rot} \, \boldsymbol{u}_h - \omega_h \big\} \, \psi_e \, L(\gamma_e) \, + \, \int_{w_e} (\omega_h - \omega) \, \psi_e \, L(\gamma_e) \, + \, \int_{w_e} \omega \, \psi_e \, L(\gamma_e) \, . \tag{4.38}$$

In turn, recalling from Theorem 2.1 that $\omega = \mathrm{rot} \, \boldsymbol{u}$ in Ω, which ensures that $\boldsymbol{u} \cdot \boldsymbol{t}$ is continuous across the edges of $\mathcal{E}_h(\Omega)$, we can integrate by parts in w_e so that, using that ψ_e vanishes on ∂w_e, we find that

$$\int_{w_e} \omega \, \psi_e \, L(\gamma_e) \, = \, \int_{w_e} \mathrm{rot} \, \boldsymbol{u} \, \psi_e \, L(\gamma_e) \, = \, \int_{w_e} \boldsymbol{u} \cdot \mathbf{curl} \left\{ \psi_e \, L(\gamma_e) \right\} .$$

In this way, replacing the foregoing equality into (4.38), and then the resulting expression into (4.37), we arrive at

$$\begin{aligned} \|\gamma_e\|_{0,e}^2 \, \leq \, c_2 \Bigg\{ &\int_{w_e} \big\{ \mathrm{rot} \, \boldsymbol{u}_h - \omega_h \big\} \, \psi_e \, L(\gamma_e) \, + \, \int_{w_e} (\omega_h - \omega) \, \psi_e \, L(\gamma_e) \\ &+ \quad \int_{w_e} (\boldsymbol{u} - \boldsymbol{u}_h) \cdot \mathbf{curl} \left\{ \psi_e \, L(\gamma_e) \right\} \Bigg\} . \end{aligned} \tag{4.39}$$

Next, applying the Cauchy-Schwarz inequality, the inverse estimate (4.24), (4.23), and the fact that $h_e \leq h_T$ for each $T \subseteq w_e$, we deduce from (4.39) that

$$\begin{aligned} \|\gamma_e\|_{0,e}^2 \, &\leq \, C \sum_{T \subseteq w_e} \Big\{ \| \mathrm{rot} \, \boldsymbol{u}_h - \omega_h\|_{0,T} \, + \, \|\omega - \omega_h\|_{0,T} \, + \, h_T^{-1} \, \|\boldsymbol{u} - \boldsymbol{u}_h\|_{0,T} \Big\} \, \|\psi_e \, L(\gamma_e)\|_{0,T} \\ &\leq \, C \sum_{T \subseteq w_e} \Big\{ h_e^{1/2} \, \| \mathrm{rot} \, \boldsymbol{u}_h - \omega_h\|_{0,T} \, + \, h_e^{1/2} \, \|\omega - \omega_h\|_{0,T} \, + \, h_T^{-1/2} \, \|\boldsymbol{u} - \boldsymbol{u}_h\|_{0,T} \Big\} \, \|\gamma_e\|_{0,e} \, , \end{aligned}$$

which yields, after some simplifications,

$$h_e \, \|\gamma_e\|_{0,e}^2 \, \leq \, C \sum_{T \subseteq w_e} \Big\{ h_T^2 \, \| \mathrm{rot} \, \boldsymbol{u}_h - \omega_h\|_{0,T}^2 \, + \, h_T^2 \, \|\omega - \omega_h\|_{0,T}^2 \, + \, \|\boldsymbol{u} - \boldsymbol{u}_h\|_{0,T}^2 \Big\} \, .$$

This inequality and the efficiency estimate for $h_T^2 \, \| \mathrm{rot} \, \boldsymbol{u}_h - \omega_h\|_{0,T}^2$ (cf. Lemma 4.11) imply (4.36) and complete the proof. □

Lemma 4.16. *There exists $C > 0$, independent of h, such that*

$$h_e \, \|\boldsymbol{a} \cdot \boldsymbol{t} - \boldsymbol{u}_h \cdot \boldsymbol{t}\|_{0,e}^2 \, \leq \, C \left\{ \|\boldsymbol{u} - \boldsymbol{u}_h\|_{0,T_e}^2 \, + \, h_{T_e}^2 \, \|\omega - \omega_h\|_{0,T_e}^2 \right\} \qquad \forall \, e \in \mathcal{E}_h(\Sigma) \, , \tag{4.40}$$

where T_e is the triangle of $\mathcal{T}_h$ having e as an edge.

Proof. Given $e \in \mathcal{E}_h(\Sigma)$, we let T_e be the triangle of $\mathcal{T}_h$ having e as an edge, and set $\gamma_e := \boldsymbol{a} \cdot \boldsymbol{t} - \boldsymbol{u}_h \cdot \boldsymbol{t}$ on e. Then, applying (4.22), employing the extension operator $L : C(e) \to C(T_e)$, and using that $\boldsymbol{u} \cdot \boldsymbol{t} = \boldsymbol{a} \cdot \boldsymbol{t}$ on Σ, we obtain

$$\|\gamma_e\|_{0,e}^2 \, \leq \, c_2 \, \|\psi_e^{1/2} \, \gamma_e\|_{0,e}^2 \, = \, c_2 \int_e \psi_e \, \gamma_e \, (\boldsymbol{a} \cdot \boldsymbol{t} - \boldsymbol{u}_h \cdot \boldsymbol{t}) \, = \, c_2 \int_{\partial T_e} \psi_e \, L(\gamma_e) \, (\boldsymbol{u} \cdot \boldsymbol{t} - \boldsymbol{u}_h \cdot \boldsymbol{t}) \, . \tag{4.41}$$

Next, integrating by parts, employing from Theorem 2.1 that $\omega = \operatorname{rot} \boldsymbol{u}$, and adding and substracting ω_h, we find that

$$\begin{aligned} \int_{\partial T_e} \psi_e \, L(\gamma_e) \, (\boldsymbol{u} \cdot \boldsymbol{t} - \boldsymbol{u}_h \cdot \boldsymbol{t}) \, &= \, - \int_{T_e} \mathbf{curl} \left\{ \psi_e \, L(\gamma_e) \right\} (\boldsymbol{u} - \boldsymbol{u}_h) \, + \, \int_{T_e} \psi_e \, L(\gamma_e) \left\{ \operatorname{rot} \boldsymbol{u} - \operatorname{rot} \boldsymbol{u}_h \right\} \\ &= \, - \int_{T_e} \mathbf{curl} \left\{ \psi_e \, L(\gamma_e) \right\} (\boldsymbol{u} - \boldsymbol{u}_h) \, + \, \int_{T_e} \psi_e \, L(\gamma_e) \left\{ \omega - \omega_h \right\} \, - \, \int_{T_e} \psi_e \, L(\gamma_e) \left\{ \operatorname{rot} \boldsymbol{u}_h - \omega_h \right\} . \end{aligned}$$

Thus, replacing the foregoing identity back into (4.41), and employing the Cauchy-Schwarz inequality, the inverse estimate (4.24), and (4.23), we deduce that

$$\|\gamma_e\|_{0,e}^2 \, \leq \, C \left\{ h_{T_e}^{-1} \, \|\boldsymbol{u} - \boldsymbol{u}_h\|_{0,T_e} \, + \, \|\omega - \omega_h\|_{0,T_e} \, + \, \|\operatorname{rot} \boldsymbol{u}_h - \omega_h\|_{0,T_e} \right\} h_e^{1/2} \, \|\gamma_e\|_{0,e} \, ,$$

which, after minor manipulations, gives

$$h_e \, \|\gamma_e\|_{0,e}^2 \, \leq \, C \left\{ \|\boldsymbol{u} - \boldsymbol{u}_h\|_{0,T_e}^2 \, + \, h_{T_e}^2 \, \|\omega - \omega_h\|_{0,T_e}^2 \, + \, h_{T_e}^2 \, \|\operatorname{rot} \boldsymbol{u}_h - \omega_h\|_{0,T_e}^2 \right\} . \tag{4.42}$$

Finally, it is easy to see that (4.42) and the efficiency estimate for $h_T^2 \, \|\operatorname{rot} \boldsymbol{u}_h - \omega_h\|_{0,T}^2$ (cf. Lemma 4.11) imply (4.40), which ends the proof. □

Consequently, the efficiency of $\boldsymbol{\theta}$ follows straightforwardly from the estimates (4.19) and (4.20), Lemma 4.11, and Lemmata 4.13 throughout 4.16. Similarly, in order to complete the efficiency estimate for $\boldsymbol{\vartheta}$, we just need to provide the corresponding upper bounds for the three remaining terms in (4.2). To this end, we now state the following preliminary result, which is the analogue of Lemma 4.12 when involving div and normal jump instead of rot and tangential jump, respectively.

Lemma 4.17. *Let $\boldsymbol{\rho}_h \in \mathbf{L}^2(\Omega)$ be a piecewise polynomial of degree $k \geq 0$ on each $T \in \mathcal{T}_h$, and let $\boldsymbol{\rho} \in \mathbf{L}^2(\Omega)$ be such that $\operatorname{div}\{\boldsymbol{\rho}\} = 0$ in Ω. Then, there exist c, $\widetilde{c} > 0$, independent of h, such that*

$$h_T^2 \, \|\operatorname{div} \{\boldsymbol{\rho}_h\}\|_{0,T}^2 \, \leq \, c \, \|\boldsymbol{\rho} - \boldsymbol{\rho}_h\|_{0,T}^2 \qquad \forall \, T \in \mathcal{T}_h \, , \tag{4.43}$$

and

$$h_e \, \|[\boldsymbol{\rho}_h \cdot \boldsymbol{n}]\|_{0,e}^2 \, \leq \, \widetilde{c} \, \|\boldsymbol{\rho} - \boldsymbol{\rho}_h\|_{0,w_e}^2 \qquad \forall \, e \in \mathcal{E}_h(\Omega) \, . \tag{4.44}$$

Proof. It follows from slight modifications of the proofs of [6, Lemmata 4.5 and 4.6]. We omit further details. □

The foregoing lemma allows us to establish the following efficiency estimates for $\boldsymbol{\vartheta}$.

Lemma 4.18. *There exist C_1, $C_2 > 0$, independent of h, such that*

$$h_T^2 \, \|\mathrm{div}\big\{\mathbf{r}(\boldsymbol{u}_h, p_h)\big\}\|_{0,T}^2 \, \leq \, C_1 \, \Big\{ \|\boldsymbol{u} - \boldsymbol{u}_h\|_{0,T}^2 \, + \, |p - p_h|_{1,T}^2 \Big\} \qquad \forall \, T \in \mathcal{T}_h \, , \tag{4.45}$$

and

$$h_e \, \|[\mathbf{r}(\boldsymbol{u}_h, p_h) \cdot \boldsymbol{n}]\|_{0,e}^2 \, \leq \, C_2 \, \Big\{ \|\boldsymbol{u} - \boldsymbol{u}_h\|_{0,w_e}^2 \, + \, |p - p_h|_{1,w_e}^2 \Big\} \qquad \forall \, e \in \mathcal{E}_h(\Omega) \, . \tag{4.46}$$

Proof. Since $\mathrm{div}\, \mathbf{curl}\, \omega = 0$ in Ω and, according to Theorem 2.1, $\nu \, \mathbf{curl}\, \omega = \boldsymbol{f} - \sigma \boldsymbol{u} - \nabla p$ in Ω, it suffices to apply Lemma 4.17 to $\boldsymbol{\rho} = \nu \, \mathbf{curl}\, \omega$ and $\boldsymbol{\rho}_h = \mathbf{r}(\boldsymbol{u}_h, p_h)$, and then employ the triangle inequality. □

We conclude our efficiency analysis for $\boldsymbol{\vartheta}$ with the following result.

Lemma 4.19. *There exists $C > 0$, independent of h, such that*

$$h_e \, \|\mathbf{r}(\boldsymbol{u}_h, p_h) \cdot \boldsymbol{n}\|_{0,e}^2 \, \leq \, C \, \Big\{ \|\boldsymbol{u} - \boldsymbol{u}_h\|_{0,T_e}^2 \, + \, |p - p_h|_{1,T_e}^2 \Big\} \qquad \forall \, e \in \mathcal{E}_h(\Gamma) \, , \tag{4.47}$$

where T_e is the triangle of $\mathcal{T}_h$ having e as an edge.

Proof. It follows analogously to the proof of Lemma 4.14. In fact, given $e \in \mathcal{E}_h(\Gamma)$ we let T_e be the triangle of $\mathcal{T}_h$ having e as an edge, and set $\gamma_e := \mathbf{r}(\boldsymbol{u}_h, p_h) \cdot \boldsymbol{n}$ on e. Since $\omega = 0$ on Γ (cf. Theorem 2.1), there holds $\mathbf{curl}\, \omega \cdot \boldsymbol{n} = \nabla \omega \cdot \boldsymbol{t} = 0$ on Γ, and hence

$$\mathbf{r}(\boldsymbol{u}_h, p_h) \cdot \boldsymbol{n} = \big\{ \mathbf{r}(\boldsymbol{u}_h, p_h) - \nu \, \mathbf{curl}\, \omega \big\} \cdot \boldsymbol{n} \quad \text{on} \quad e \, .$$

Then, applying (4.22) and the extension operator $L : C(e) \to C(T_e)$, we obtain that

$$\begin{aligned} \|\gamma_e\|_{0,e}^2 \, &\leq \, c_2 \, \|\psi_e^{1/2} \, \gamma_e\|_{0,e}^2 \, = \, c_2 \, \int_e \psi_e \, \gamma_e \, \big\{ \mathbf{r}(\boldsymbol{u}_h, p_h) \cdot \boldsymbol{n} \big\} \\ &= \quad c_2 \, \int_{\partial T_e} \psi_e \, L(\gamma_e) \, \Big\{ \big\{ \mathbf{r}(\boldsymbol{u}_h, p_h) - \nu \, \mathbf{curl}\, \omega \big\} \cdot \boldsymbol{n} \Big\} \, . \end{aligned} \tag{4.48}$$

Now, integrating by parts and using that $\mathrm{div}\big\{ \mathbf{curl}\, \omega \big\} = 0$ in Ω, we find that

$$\begin{aligned} &\int_{\partial T_e} \psi_e \, L(\gamma_e) \, \Big\{ \big\{ \mathbf{r}(\boldsymbol{u}_h, p_h) - \nu \, \mathbf{curl}\, \omega \big\} \cdot \boldsymbol{n} \Big\} \\ = \, &\int_{T_e} \nabla(\psi_e \, L(\gamma_e)) \cdot \big\{ \mathbf{r}(\boldsymbol{u}_h, p_h) - \nu \, \mathbf{curl}\, \omega \big\} \, + \, \int_{T_e} \psi_e \, L(\gamma_e) \, \mathrm{div} \, \big\{ \mathbf{r}(\boldsymbol{u}_h, p_h) \big\} \, . \end{aligned} \tag{4.49}$$

On the other hand, using that $0 \leq \psi_e \leq 1$ and (4.23), we have that

$$\|\psi_e \, L(\gamma_e)\|_{0,T_e} \, \leq \, \|\psi_e^{1/2} \, L(\gamma_e)\|_{0,T_e} \, \leq \, c \, h_e^{1/2} \|\gamma_e\|_{0,e} \, . \tag{4.50}$$

Hence, applying the Cauchy-Schwarz inequality and the inverse estimate (4.24), and recalling from Theorem 2.1 that $\nu \, \mathbf{curl}\, \omega = \boldsymbol{f} - \sigma \boldsymbol{u} - \nabla p$ in Ω, we deduce from (4.48), (4.49), and (4.50) that

$$\|\gamma_e\|_{0,e}^2 \, \leq \, C \, \Big\{ h_{T_e}^{-1} \, \Big\{ \|\boldsymbol{u} - \boldsymbol{u}_h\|_{0,T_e} + |p - p_h|_{1,T_e} \Big\} \, + \, \|\mathrm{div} \, \big\{ \mathbf{r}(\boldsymbol{u}_h, p_h) \big\}\|_{0,T_e} \Big\} \, h_e^{1/2} \, \|\gamma_e\|_{0,e} \, ,$$

which yields

$$h_e \, \|\gamma_e\|_{0,e}^2 \, \leq \, C \, \Big\{ \|\boldsymbol{u} - \boldsymbol{u}_h\|_{0,T_e}^2 \, + \, |p - p_h|_{1,T_e}^2 \, + \, h_{T_e}^2 \, \|\mathrm{div} \, \big\{ \mathbf{r}(\boldsymbol{u}_h, p_h) \big\}\|_{0,T_e}^2 \Big\} \, ,$$

where we have also employed that $h_e \leq h_{T_e}$. The foregoing inequality and the upper bound for $h_{T_e}^2 \, \|\mathrm{div}\big\{\mathbf{r}(\boldsymbol{u}_h, p_h)\big\}\|_{0,T_e}^2$ (cf. Lemma 4.18) imply (4.47) and complete the proof. □

We end this section by remarking that the efficiency of $\boldsymbol{\vartheta}$ follows from the corresponding estimate of $\boldsymbol{\theta}$ together with Lemmata 4.18 and 4.19.

5 Numerical experiments

We now turn to the presentation of selected numerical examples confirming our theoretical findings. The solutions of the unsymmetric linear systems involved in the discretization of the model problem are computed with the multifrontal massively parallel sparse direct solver MUMPS. Given the solution $(\boldsymbol{u}, \omega, p) \in \mathbf{H}_\Gamma(\mathrm{div};\Omega) \times \mathrm{H}^1_\Gamma(\Omega) \times \mathrm{H}^1_\Sigma(\Omega)$ of our continuous augmented formulation (2.4), we measure the accuracy of the numerical scheme by the errors

$$e(\boldsymbol{u}) := \|\boldsymbol{u} - \boldsymbol{u}_h\|_{\mathrm{div},\Omega},\ e(\omega) := \|\omega - \omega_h\|_{1,\Omega},\ e(p) := \|p - p_h\|_{1,\Omega}\,,$$

where $(\boldsymbol{u}_h, \omega_h, p_h) \in \mathbb{H}_h$ is the solution of the augmented Galerkin scheme (3.2). In turn, the associated observed convergence rates are computed as

$$r(\cdot) := \frac{\log(e(\cdot)/\hat{e}(\cdot))}{\log(h/\hat{h})},$$

where e and $\hat{e}$ denote errors associated to two consecutive meshes of sizes h and $\hat{h}$. To this respect, in what follows N denotes the number of degrees of freedom associated to a given triangulation. Bear in mind that the above notations are also employed below in Section 5.2 for the case of a reference solution $(\boldsymbol{u}_{\mathrm{ref}}, \omega_{\mathrm{ref}}, p_{\mathrm{ref}})$ instead of $(\boldsymbol{u}, \omega, p)$. Furthermore, concerning the stabilization coefficients, in Examples 1 throughout 3 below we consider the optimal values described at the end of Section 3, that is $\kappa_1 = \frac{\nu}{2\sigma}$, $\kappa_2 = \frac{1}{2\sigma}$, and $\kappa_3 = \frac{\sigma}{2}$, where σ and ν are the model parameters.

5.1 Example 1: Convergence tests against analytical solutions

We consider a square-shaped closed cavity $\Omega = (0,1)^2$ where the boundary is split into Γ (bottom and right lids of the square) and Σ (top and left sides of the square).

A sequence of uniformly refined meshes is employed to compute these errors and rates with respect to the following exact solutions of (1.1)

$$\boldsymbol{u} = \begin{pmatrix} -\sin(\pi x_1)\cos(\pi x_2) \\ \sin(\pi x_2)\cos(\pi x_1) \end{pmatrix}, \quad \omega = -2\pi \sin(\pi x_2)\sin(\pi x_1), \quad p = x_1^2(1 - x_2^2),$$

satisfying the set of boundary data

$$\begin{cases} \omega = 0,\ \boldsymbol{u}\cdot\boldsymbol{n} = 0 & \text{on } \Gamma, \\ p = 0,\ \boldsymbol{u}\cdot\boldsymbol{t} = \sin(\pi x_1)\cos(\pi x_2)n_2 + \sin(\pi x_2)\cos(\pi x_1)n_1 & \text{on } \Sigma. \end{cases}$$

We consider the model parameters $\sigma = 0.1$ and $\nu = 0.01$. The error history and the effectivity indexes for $\boldsymbol{\theta}$ and $\boldsymbol{\vartheta}$ are presented in Table 5.1 for two finite element families using $\mathbf{RT}_0 - P_1 - P_1$ ($k = 0$) and $\mathbf{RT}_1 - P_2 - P_2$ ($k = 1$) approximations for velocity, vorticity and pressure. The table shows that the accuracy of the schemes approaches asymptotically an order $O(h^{k+1})$ for the vorticity and pressure in the $\mathrm{H}^1(\Omega)-$norm and for the velocity in the $\mathbf{H}(\mathrm{div};\Omega)-$norm. In addition, the last two columns of Table 5.1 show that $\mathtt{eff}(\boldsymbol{\theta})$ and $\mathtt{eff}(\boldsymbol{\vartheta})$ remain always bounded, which confirms the reliability and efficiency of both a posteriori error estimators. Contour plots of the approximations obtained on an intermediate mesh with 155652 cells and 77827 vertices with the lowest order family (representing roughly half a million degrees of freedom) are reported in Figure 5.1.

N	h	$e(\omega)$	$r(\omega)$	$e(\boldsymbol{u})$	$r(\boldsymbol{u})$	$e(p)$	$r(p)$	$\mathtt{eff}(\boldsymbol{\theta})$	$\mathtt{eff}(\boldsymbol{\vartheta})$
$\mathbf{RT}_0 - P_1 - P_1$ finite elements									
34	0.707107	8.663562	–	1.128531	–	0.566262	–	3.394480	2.348912
289	0.202031	3.042580	0.835291	0.165443	1.532650	0.134389	1.148111	2.916250	2.372894
1378	0.088388	1.361391	0.972808	0.069581	1.047711	0.057595	1.024953	2.773871	2.302962
4381	0.048766	0.754373	0.992713	0.038304	1.003762	0.031624	1.008094	2.741535	2.284435
10858	0.030743	0.476180	0.997276	0.024144	1.000363	0.019908	1.003083	2.730383	2.277252
22849	0.021107	0.327081	0.998753	0.016576	0.999982	0.013661	1.001377	2.725384	2.273743
42874	0.015371	0.238253	0.999348	0.012072	0.999939	0.009947	1.000691	2.722743	2.271742
73933	0.011687	0.181164	0.999625	0.009179	0.999947	0.007562	1.000380	2.721174	2.270497
119506	0.009183	0.142352	0.999768	0.007212	0.999959	0.005941	1.000236	2.720171	2.269654
183553	0.007404	0.114783	0.999849	0.005815	0.999969	0.004790	1.000146	2.719482	2.269063
270514	0.006095	0.094499	0.999897	0.004787	0.999977	0.003943	1.000109	2.718991	2.268634
385309	0.005105	0.079148	0.999928	0.004009	0.999982	0.003302	1.000070	2.719032	2.268943
533338	0.004338	0.067252	0.999947	0.003407	0.999986	0.002806	1.000051	2.719193	2.269012
720481	0.003731	0.057847	0.999966	0.002361	0.999991	0.002412	1.000030	2.719145	2.269160
$\mathbf{RT}_1 - P_2 - P_2$ finite elements									
98	0.707107	2.753852	–	0.217709	–	0.097066	–	0.180569	0.167872
968	0.202031	0.266276	1.864870	0.014382	2.168913	0.006625	2.142810	0.496039	0.394618
4802	0.088388	0.052312	1.968457	0.002687	2.029184	0.001268	1.999322	0.496915	0.394605
15488	0.048766	0.016037	1.988121	8.8152e-4	2.004256	3.8728e-4	1.993636	0.503835	0.406301
38642	0.030743	0.006391	1.993864	3.2410e-4	1.999490	1.5439e-4	1.995983	0.497461	0.397375
81608	0.021107	0.003017	1.996242	1.5298e-4	1.998673	7.2847e-5	1.997344	0.491595	0.391526
153458	0.015371	0.001601	1.997451	8.1170e-5	1.998665	3.8658e-5	1.998127	0.501924	0.411273
264992	0.011687	9.2632e-4	1.998167	4.6939e-5	1.998834	2.2357e-5	1.998628	0.484082	0.384070
428738	0.009183	5.7205e-4	1.998650	2.8985e-5	1.999021	1.3805e-5	1.998921	0.509795	0.406397
658952	0.007404	3.7197e-4	1.998927	1.8846e-5	1.999152	8.9766e-6	1.999143	0.505238	0.405025
971618	0.006095	2.3062e-4	1.999289	9.1407e-6	1.999378	4.0412e-6	1.999587	0.504564	0.404027
1384448	0.005105	1.0793e-4	1.999712	4.8532e-6	1.999629	2.0237e-6	1.999764	0.504027	0.403340
1916882	0.004338	7.2521e-5	1.999934	2.4129e-6	1.999917	1.0168e-6	1.999902	0.503735	0.404102

Table 5.1: Example 1: Convergence tests against analytical solutions employing $\mathbf{RT}_0 - P_1 - P_1$ (top rows) and $\mathbf{RT}_1 - P_2 - P_2$ (bottom rows) FE approximations of velocity-vorticity-pressure computed on a sequence of uniformly refined triangulations of the unit square.

5.2 Example 2: Experimental convergence with respect to a reference solution

Our next test focuses on the mixed $\mathbf{BDM}_1 - P_1 - P_1$ approximations of problem (1.1) defined on the nonconvex L-shaped domain $\Omega = (-1,1)^2 \setminus (0,1)^2$. The forcing term is $\boldsymbol{f} = (x_2, 0)^{\mathtt{t}}$ and the following boundary conditions are applied on $\Gamma = \partial\Omega$ (see e.g. [2])

$$\boldsymbol{u}\cdot\boldsymbol{n} = \begin{cases} x_2^2 - 1 & \text{if } x_1 = -1,\ -1 \le x_2 \le 1, \\ -8x_2(1+x_2) & \text{if } x_1 = 1,\ -1 \le x_2 \le 0, \\ 0 & \text{elsewhere on } \Gamma, \end{cases}$$

$$\omega = \omega_0 = 0 \quad \text{on } \Gamma.$$

The model parameters are $\sigma = 10$ and $\nu = 1$. Even for a smooth imposed normal velocity on the boundary, we expect the nonconvexity of the domain to yield high velocity gradients and degenerate convergence to the exact solution. This is verified in Figure 5.2 where approximate velocity components, vorticity and pressure are displayed for a mesh of 57898 elements and 28950 vertices, and from

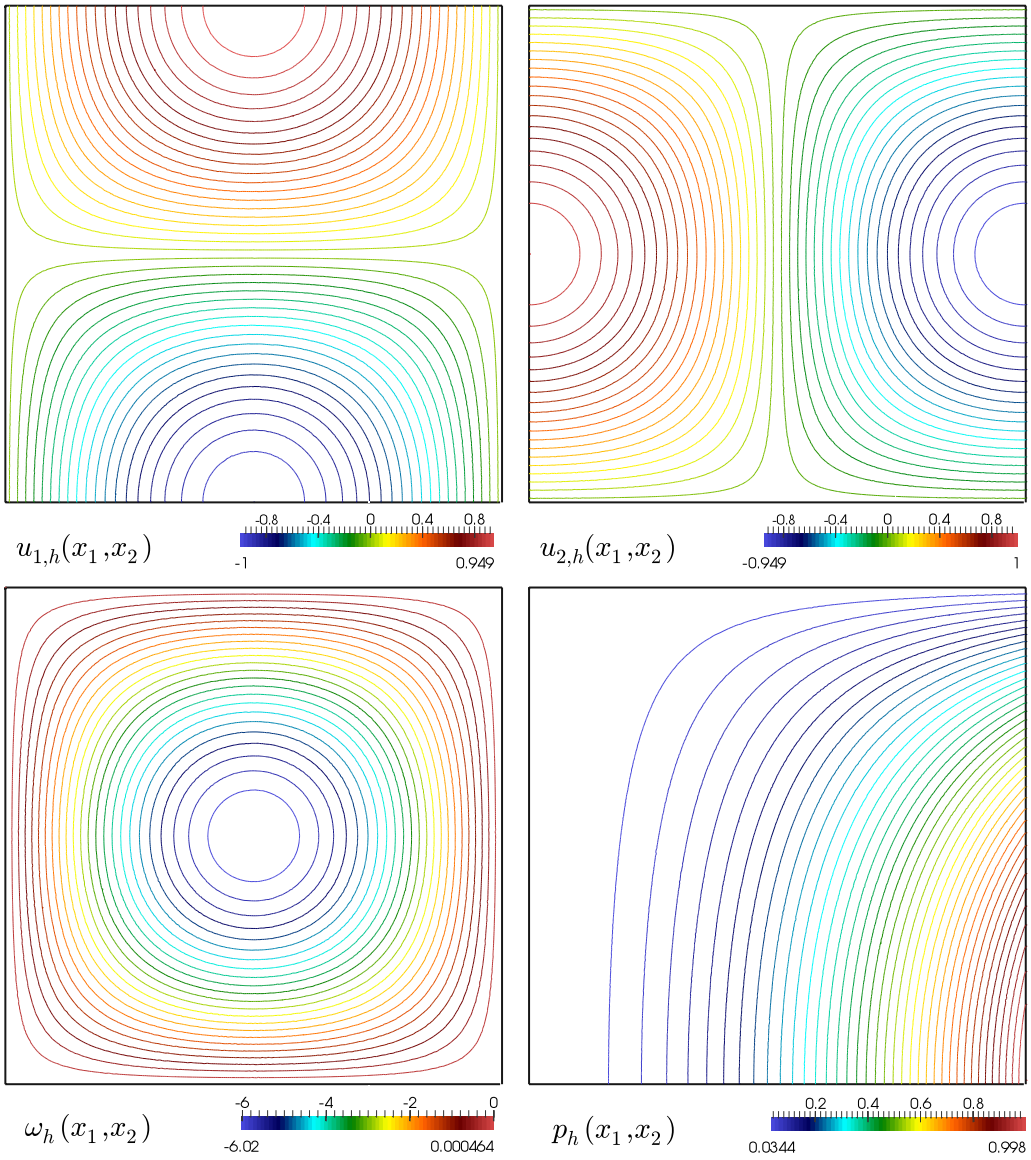

Figure 5.1: Example 1: Contour plots of the approximated velocity components (top), vorticity (bottom left), and pressure (bottom right), computed with an augmented $\mathbf{RT}_0 - P_1 - P_1$ family for the Brinkman problem on a structured mesh of 155652 elements and 77827 vertices.

Table 5.2, where experimental errors (computed with respect to a fine reference solution) are reported, exhibiting suboptimal convergence rates.

5.3 Example 3: A posteriori error estimation and mesh adaptation

Our third example illustrates the properties of the error estimator introduced and analyzed in Section 4. Again, the domain corresponds to the nonconvex L-shaped region $\Omega = (-1,1)^2 \setminus (0,1)^2$, on which the

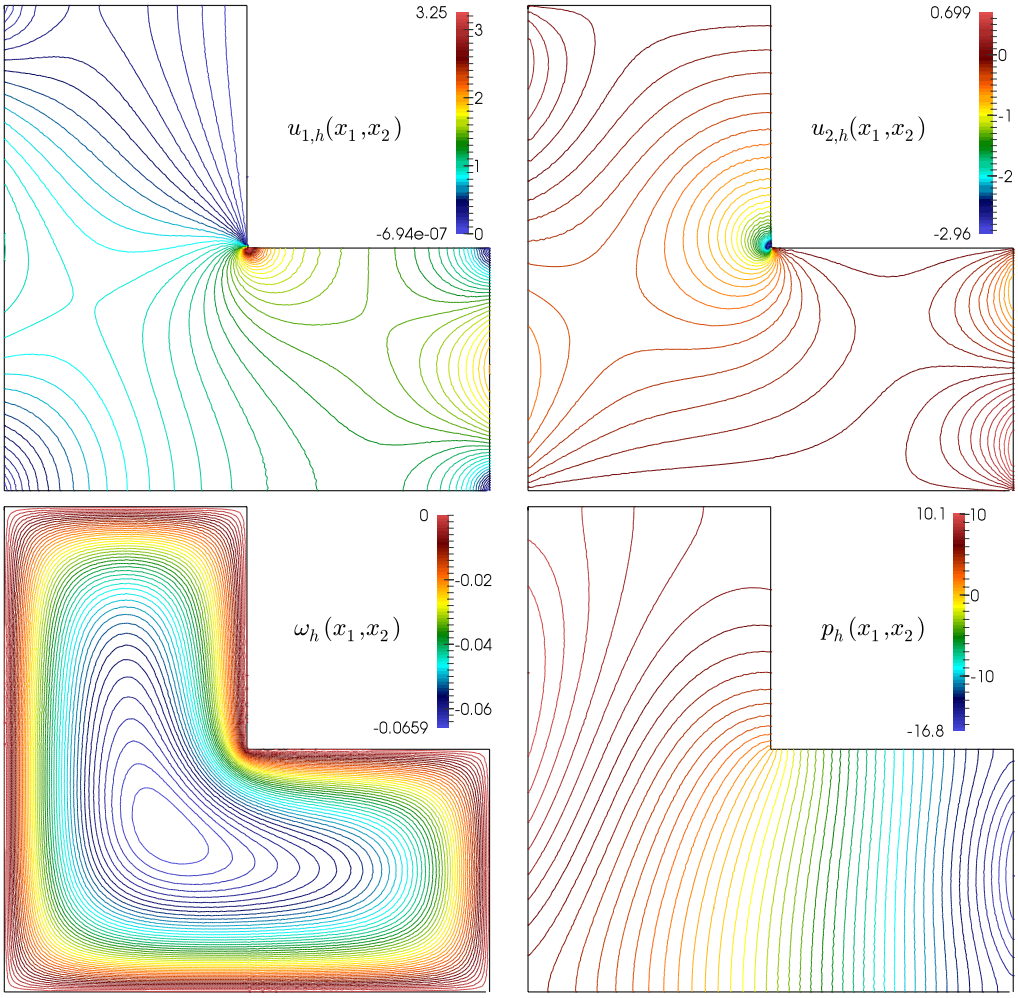

Figure 5.2: Example 2: Contour plots of the approximated velocity components (top), vorticity (bottom left), and pressure (bottom right), computed with an augmented $\mathbf{BDM}_1 - P_1 - P_1$ family for the Brinkman problem on an unstructured triangulation of the L-shaped domain.

following exact solutions of (1.1) can be considered

$$\boldsymbol{u} = \begin{pmatrix} -\sin(x_1)\cos(x_2) \\ \sin(x_2)\cos(x_1) \end{pmatrix}, \quad \omega = -2\sin(x_2)\sin(x_1), \quad p = \frac{1-x_1}{(x_1-x_a)^2+(x_2-x_b)^2},$$

with $x_a = x_b = 0.05$, and forcing terms are constructed according to these functions. Model parameters are chosen as $\sigma = 1$ and $\nu = 0.01$. The boundary Γ is the inner corner of the the domain ($x_1 = 0$ and $x_2 = 0$) where we impose $w = 0$ and $\boldsymbol{u}\cdot\boldsymbol{n} = 0$, whereas Σ is formed by the remaining segments of $\partial\Omega$ where we set $p = 0$ and $\boldsymbol{u}\cdot\boldsymbol{t} = \sin(x_2)\cos(x_1)t_2 - \sin(x_1)\cos(x_2)t_1$. We analyze the accuracy of the finite element approximation, first on a sequence of uniformly refined grids, and secondly on meshes adaptively refined according to the global a posteriori error estimators (4.3). Mesh refinement was implemented according to the well-known *blue-green* strategy (see details in e.g. [43, 20, 32]). For this example we compute the individual convergence rates as

$$r(\cdot) := -2\log(e(\cdot)/\hat{e}(\cdot))[\log(N/\hat{N})]^{-1},$$

N	h	$e(\omega_{\rm ref})$	$r(\omega_{\rm ref})$	$e(\boldsymbol{u}_{\rm ref})$	$r(\boldsymbol{u}_{\rm ref})$	$e(p_{\rm ref})$	$r(p_{\rm ref})$
42	1.414210	0.247112	–	2.335145	–	7.055480	–
130	0.750000	0.169301	0.596228	1.806842	0.814551	4.956274	0.556796
746	0.298142	0.078222	0.836976	1.475021	0.631235	2.595472	0.701229
2858	0.166875	0.038948	1.201621	0.928274	0.798003	1.578463	0.856964
8346	0.094886	0.023732	0.877510	0.560912	0.892308	1.120087	0.607639
18698	0.067183	0.016746	1.009847	0.421598	0.827015	0.823019	0.892604
37306	0.053650	0.012341	1.357252	0.261197	1.728470	0.596361	1.032152
68186	0.036060	0.009533	0.649707	0.169605	1.086827	0.466019	0.620729
114682	0.026678	0.008064	0.555524	0.103668	1.633632	0.377620	0.697997
187418	0.022005	0.006808	0.879075	0.083456	1.348910	0.303283	1.138433
278130	0.018275	0.004156	0.754791	0.064739	1.081331	0.265899	0.846078

Table 5.2: Example 2: Experimental convergence test against a reference solution $(\boldsymbol{u}_{\rm ref}, \omega_{\rm ref}, p_{\rm ref})$, employing $\mathbf{BDM}_1 - P_1 - P_1$ FE approximations of velocity-vorticity-pressure computed on a sequence of nonuniform refinements of the L-shaped domain.

where N and $\hat{N}$ denote the corresponding degrees of freedom at each triangulation, and we also define the total error, its convergence rate, and the effectivity index associated to a given global estimator $\boldsymbol{\zeta} \in \{\boldsymbol{\theta}, \boldsymbol{\vartheta}\}$ as

$$\mathtt{e} := \left\{[e(\omega)]^2 + [e(\boldsymbol{u})]^2 + [e(p)]^2\right\}^{1/2}, \quad \mathtt{r} := -2\log(\mathtt{e}/\hat{\mathtt{e}})[\log(N/\hat{N})]^{-1}, \quad \mathtt{eff}(\boldsymbol{\zeta}) := \mathtt{e}\,\boldsymbol{\zeta}^{-1}.$$

These quantities are displayed in Table 5.3, where we can observe that the total error converges sub-optimally under quasi-uniform refinement, whereas convergence rates slightly above the optimal and stable effectivity indexes are attained for both cases of adaptive mesh refinement. Approximate solutions computed with an augmented $\mathbf{RT}_0 - P_1 - P_1$ family are depicted in Figure 5.3, and some adapted meshes are presented in Figure 5.4, showing a qualitative equivalence between the two different indicators in this particular example.

5.4 Example 4: Flow in a contracting channel with a porous obstacle

We finally analyze the patterns of the flow within a channel with a sudden contraction and in the presence of a porous obstacle, as studied in e.g. [34]. For the boundary conditions we put $\Gamma = \Gamma_{\rm wall} \cup \Gamma_{\rm in} \cup \Gamma_{\rm out} \partial\Omega$ and $\Sigma = \emptyset$ (see the sketch in Figure 5.5), and specify a normal Poiseuille velocity inflow and outflow on $\Gamma_{\rm in}$ and $\Gamma_{\rm out}$, respectively (along with compatible vorticity in each case) and impose slip conditions elsewhere. That is,

$$\boldsymbol{u}\cdot\boldsymbol{n} = \begin{cases} \alpha_{\rm in} x_1(x_1 - 3/2) & \text{on } \Gamma_{\rm in}, \\ \alpha_{\rm out} x_1(x_1 - 3/5) & \text{on } \Gamma_{\rm out}, \\ 0 & \text{on } \Gamma_{\rm wall}, \end{cases} \qquad \omega = \omega_0 = \begin{cases} \alpha_{\rm in}(2x_1 - 3/2) & \text{on } \Gamma_{\rm in}, \\ \alpha_{\rm out}(2x_1 - 3/5) & \text{on } \Gamma_{\rm out}, \\ 0 & \text{on } \Gamma_{\rm wall}, \end{cases}$$

with $\alpha_{\rm in} = 2/75$, $\alpha_{\rm out} = 5/12$, ensuring that the flow rates at the inflow and outflow boundaries coincide, and we take $\nu = 1$.

We further assume that the coefficient σ (that represents the inverse permeability of the medium) is possibly discontinuous

$$\sigma(x_1, x_2) = \begin{cases} \sigma_0 + \sigma_1 & \text{on the porous obstacle,} \\ \sigma_0 & \text{otherwise,} \end{cases}$$

N	$e(\omega)$	$r(\omega)$	$e(\boldsymbol{u})$	$r(\boldsymbol{u})$	$e(p)$	$r(p)$	e	r	eff($\boldsymbol{\theta}$)	eff($\boldsymbol{\vartheta}$)
Quasi-uniform refinement										
89	92.10302	–	10.12382	–	289.6016	–	304.0633	–	1.049541	0.408742
709	252.2121	-0.96887	8.126014	0.211425	476.9278	-0.47983	539.5714	-0.55162	1.131525	0.416326
2601	42.98782	2.561512	4.570156	0.833185	428.0051	0.156683	430.1825	0.327997	1.005256	0.418037
7022	4.632165	4.476213	1.619454	2.084456	303.1442	0.693022	303.1837	0.702955	1.000183	0.418771
15617	1.218119	4.650495	1.025913	1.589383	238.2463	0.838741	238.2518	0.839119	1.000054	0.419946
30321	0.106278	5.804742	0.713606	0.863941	199.2018	0.425991	199.2025	0.426029	1.000029	0.414001
53534	0.047772	3.541487	0.466607	1.881665	161.2695	0.935575	161.2796	0.935585	1.000022	0.411894
88826	0.020123	3.345247	0.230782	2.724687	116.2435	1.266874	116.2435	0.866883	1.000015	0.416477
140517	0.014175	1.636090	0.173017	1.345333	99.00490	0.749465	99.00557	0.749462	1.000012	0.412909
206827	0.011403	1.612655	0.118302	2.816462	83.28521	1.286590	86.22232	0.856591	1.005052	0.419079
Adaptive refinement using $\boldsymbol{\theta}$										
89	91.38271	–	10.27454	–	282.7271	–	285.6762	–	1.024215	–
188	71.50388	1.175420	9.124144	0.673578	250.2252	0.299417	270.4011	0.280289	1.041294	–
504	25.70819	4.443125	5.657072	0.987094	462.3110	-0.82570	463.0594	-0.81083	1.001823	–
1016	1.418674	8.264953	1.110110	4.645723	249.7937	1.756236	249.7999	1.760776	1.000051	–
2534	0.137455	5.108032	0.274131	3.060665	110.9823	1.775375	110.9811	1.775424	1.000010	–
9204	0.104376	0.426865	0.090156	1.724353	42.56176	1.486073	42.56193	1.486076	0.999961	–
43700	0.069303	0.525783	0.039856	1.048030	16.33914	1.229231	16.33932	1.229225	0.999866	–
280832	0.047708	0.401391	0.024232	0.534934	5.900880	1.094882	5.901128	1.094853	0.999493	–
828623	0.028216	0.730731	0.016523	1.588990	2.477021	1.404517	1.565234	1.164862	1.000005	–
Adaptive refinement using $\boldsymbol{\vartheta}$										
89	91.38270	–	16.27453	–	281.7279	–	283.6763	–	–	0.198789
188	84.36767	1.277472	12.40693	1.202951	269.7647	0.202557	269.9575	0.263561	–	0.417859
512	42.30257	1.668225	4.138492	1.963533	428.4066	-0.85802	432.5095	-0.87233	–	0.416173
1203	0.245006	12.06055	0.825899	3.773178	220.0954	1.559356	220.0964	1.357074	–	0.415403
3343	0.127734	1.274562	0.188241	2.893694	88.79212	1.776354	88.79233	1.776362	–	0.416205
11663	0.101293	0.371224	0.078261	1.404779	33.09974	1.579423	33.15476	1.579393	–	0.414196
58891	0.065322	0.541827	0.036403	0.945358	12.31275	1.221414	12.31292	1.221401	–	0.415953
411923	0.047788	0.321364	0.024208	0.419442	4.463042	1.043427	4.463361	1.143036	–	0.414526
954725	0.028276	0.712833	0.017525	0.662607	3.159851	1.070844	2.725254	1.261190	–	0.415151

Table 5.3: Example 3: Convergence tests against analytical solutions employing augmented $\mathbf{RT}_0 - P_1 - P_1$ FE approximations of velocity-vorticity-pressure, computed on a sequence of quasi-uniformly refined triangulations (top rows), adaptively refined according to the estimator $\boldsymbol{\theta}$ (middle rows), and adaptively refined according to $\boldsymbol{\vartheta}$ (bottom rows), defined as in (4.3).

where $\sigma_0 = 0.001$ and $\sigma_1 \in \{0.001, 0.1, 10, 1000\}$, and focus first on the case where the permeabilities inside and outside the obstacle differ by six orders of magnitude. There we expect velocity patterns avoiding the obstacle, and vanishing of the vorticity due to a Darcy regime with constant permeability inside the obstacle. These phenomena can be indeed observed from Figure 5.6, where we plot contours of velocity components, vorticity and pressure obtained with a $\mathbf{BDM}_1 - P_1 - P_1$ approximation. The unstructured mesh consists of 125670 triangles and 62696 nodes.

Next, using the same finite element family and the same mesh, we perform a qualitative comparison of the flow patterns depending on the value of the inverse permeability σ_1. The three panels in Figure 5.7 indicate that if the difference between the permeability inside and outside the obstacle is small, the flow (velocity and vorticity) in the porous part is practically identical to the one in rest of the domain. However as σ_1 increases, the zeroth order term in the Brinkman problem is dominant and the flow gradually avoids the porous obstacle. In all cases, the stabilization parameters were chosen as

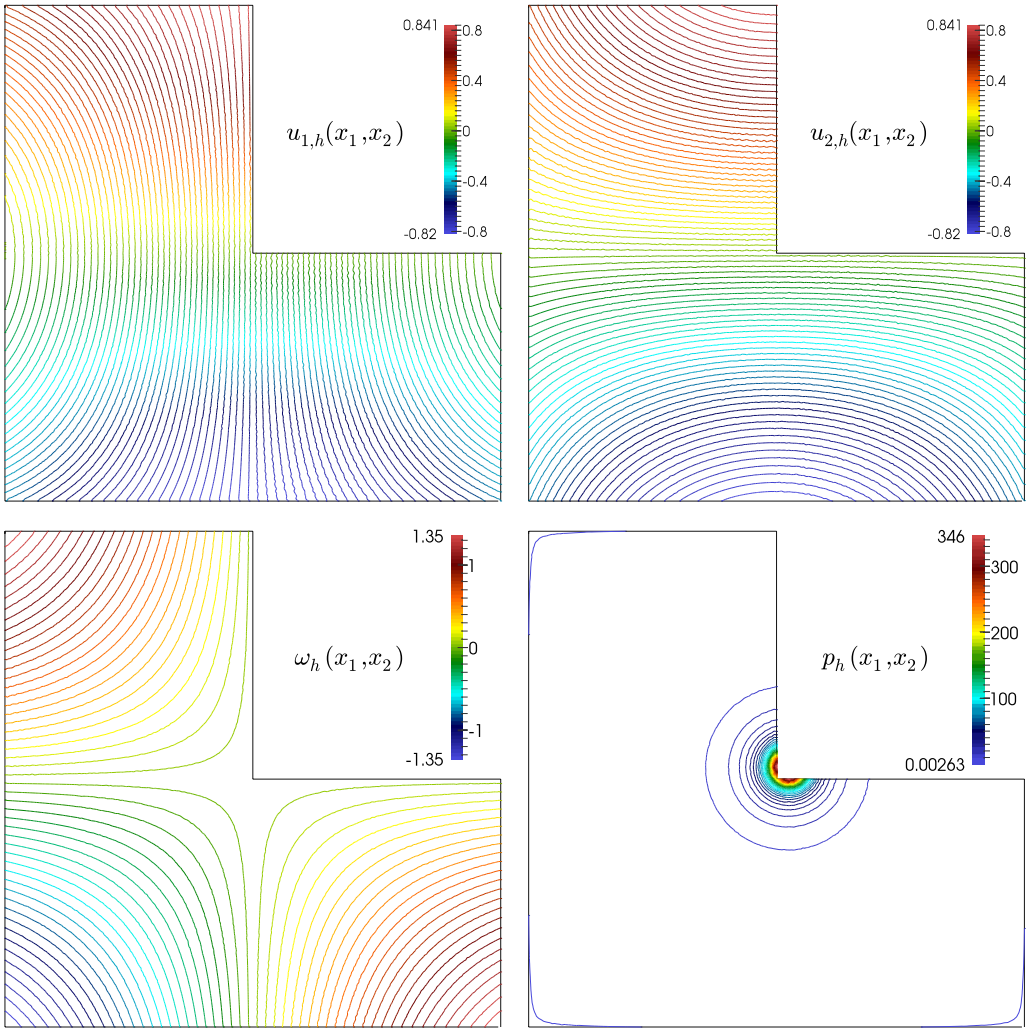

Figure 5.3: Example 3: Contour plots of the approximated velocity components (top), vorticity (bottom left), and pressure (bottom right), computed with an augmented $\mathbf{RT}_0 - P_1 - P_1$ family for the Brinkman problem on an unstructured triangulation of the L-shaped domain.

$\kappa_1 = 0.5\nu\sigma_0\sigma_1^{-2}, \kappa_2 = 0.5\sigma_0\sigma_1^{-2}, \kappa_3 = 0.5\sigma_0$. Actually, even though our analysis for the continuous and discrete augmented formulations was carried out for a constant σ, it can be straightforwardly adapted to cover Example 4, where a discontinuous coefficient accompanying the zeroth order velocity term is employed (here interpreted as the inverse permeability of the porous medium). In this case (and in the light of the proof of Lemma 2.2), it suffices to require $\sigma = \sigma(\boldsymbol{x}) \in \mathrm{L}^\infty(\Omega)$ with $0 < \sigma_{\min} \leq \sigma(\boldsymbol{x}) \leq \sigma_{\max}$ for $\boldsymbol{x} \in \mathbb{R}^2$, and so the stabilization parameters need to satisfy $0 < \kappa_1 < \frac{\nu\sigma_{\min}}{\sigma_{\max}^2}$, $0 < \kappa_2 < \frac{\sigma_{\min}}{\sigma_{\max}^2}$ and $\kappa_3 > 0$. However, similarly to the discussion at the end of Section 3, the optimal values are given by the midpoints of the intervals for κ_1 and κ_2, and $\kappa_3 \geq 0.5\sigma_{\min}$.

References

[1] M. Amara, E. Chacón Vera, and D. Trujillo, *Vorticity–velocity–pressure formulation for*

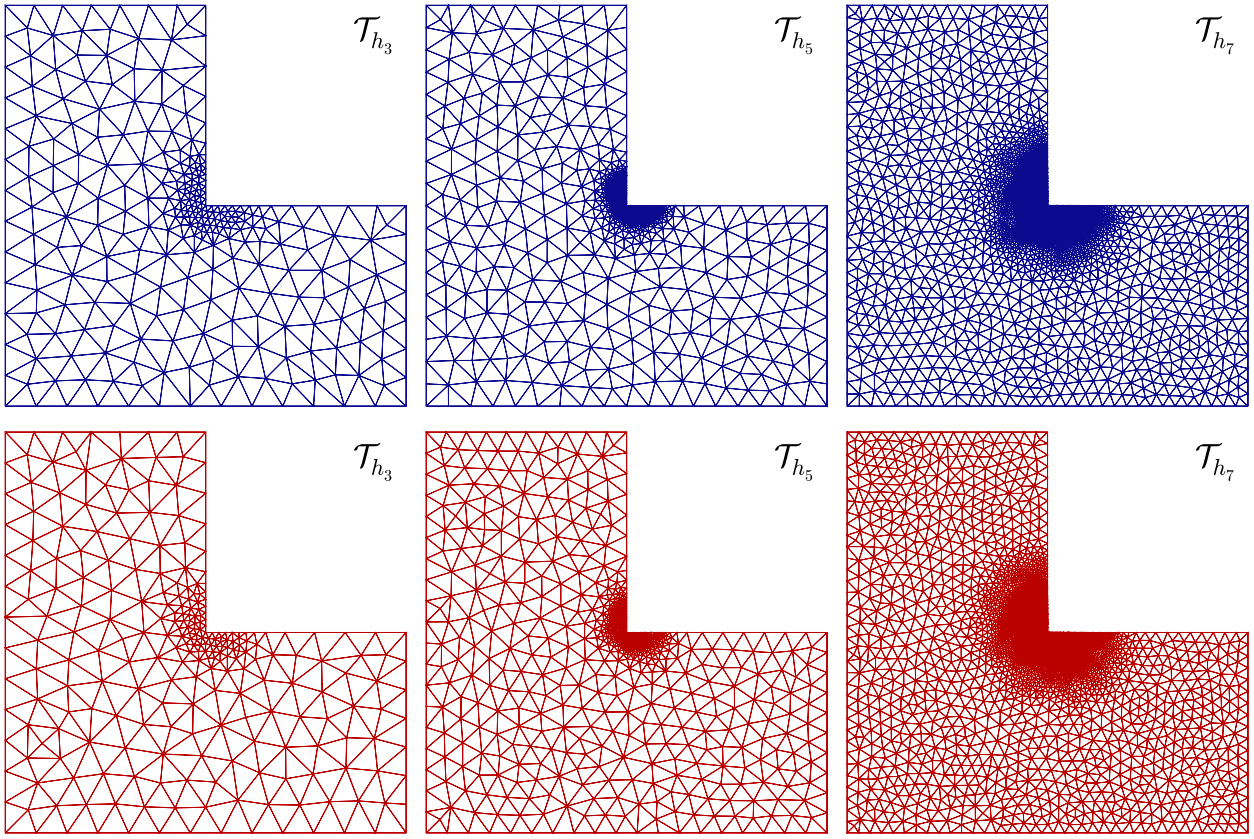

Figure 5.4: Example 3: Successively refined meshes according to the indicators $\boldsymbol{\theta}$ and $\boldsymbol{\vartheta}$ (top and bottom panels, respectively).

Stokes problem. Math. Comp., 73(248) (2004) 1673–1697.

[2] K. Amoura, C. Bernardi, and N. Chorfi, *Spectral element discretization of the vorticity, velocity and pressure formulation of the Stokes problem*. ESAIM M2AN, 40(5) (2006) 897–921.

[3] V. Anaya, D. Mora, and R. Ruiz-Baier, *An augmented mixed finite element method for the vorticity-velocity-pressure formulation of the Stokes equations*. Comput. Methods Appl. Mech. Engrg., 267 (2013) 261–274.

[4] T.P. Barrios, R. Bustinza, G. García, and E. Hernández, *On stabilized mixed methods for generalized Stokes problem based on the velocity-pseudostress formulation: a priori error estimates*. Comput. Methods Appl. Mech. Engrg., 237/240 (2012) 78–87.

[5] T.P. Barrios and G.N. Gatica, *An augmented mixed finite element method with Lagrange multipliers: a priori and a posteriori error analyses*. J. Comput. Appl. Math., 200(2) (2007) 653–676.

[6] T.P. Barrios, G.N. Gatica, G.N., M. González, and N. Heuer, *A residual based a posteriori error estimator for an augmented mixed finite element method in linear elasticity*. M2AN Math. Model. Numer. Anal., 40(5) (2006) 843–869.

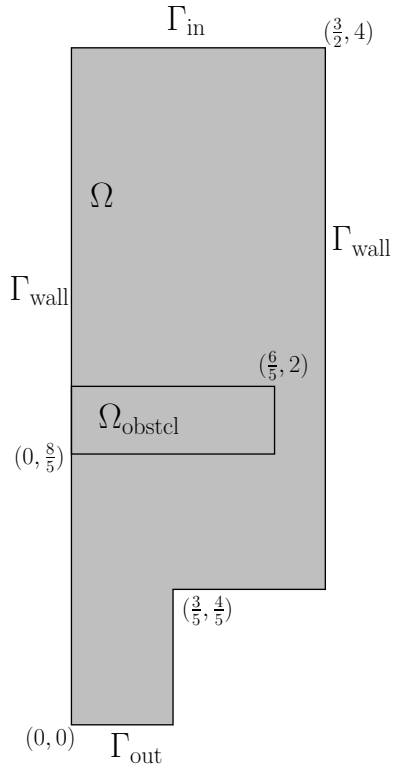

Figure 5.5: Example 4: Sketch of the domain and boundaries employed for the simulation of flow in a channel with sudden contraction.

[7] C. Bernardi and N. Chorfi, *Spectral discretization of the vorticity, velocity, and pressure formulation of the Stokes problem*. SIAM J. Numer. Anal., 44(2) (2007) 826–850.

[8] P.V. Bochev, *Analysis of least-squares finite element methods for the Navier–Stokes equations*. SIAM J. Numer. Anal., 34(5) (1997) 1817–1844.

[9] P.V. Bochev and M. Gunzburger, *Least-Squares finite element methods*. Volume 166 of Applied Mathematical Sciences. Springer Verlag, 2009.

[10] F. Brezzi and M. Fortin, *Mixed and Hybrid Finite Element Methods*. Springer Verlag, New York, 1991.

[11] E. Burman and P. Hansbo, *Edge stabilization for the generalized Stokes problem: a continuous interior penalty method*. Comput. Meth. Appl. Mech. Engrg., 195(19–22) (2006) 2393–2410.

[12] R. Bustinza, G.N. Gatica, and M. González, *A mixed finite element method for the generalized Stokes problem*. Internat. J. Numer. Methods Fluids, 49(8) (2005) 877–903.

[13] C. Carstensen, *A-posteriori error estimate for the mixed finite element method*. Mathematics of Computation, 66(218) (1997) 465–476.

[14] C.L. Chang and B.-N. Jiang, *An error analysis of least-squares finite element method of velocity-pressure-vorticity formulation for the Stokes problem*. Comput. Meth. Appl. Mech. Engrg., 84(3) (1990) 247–255.

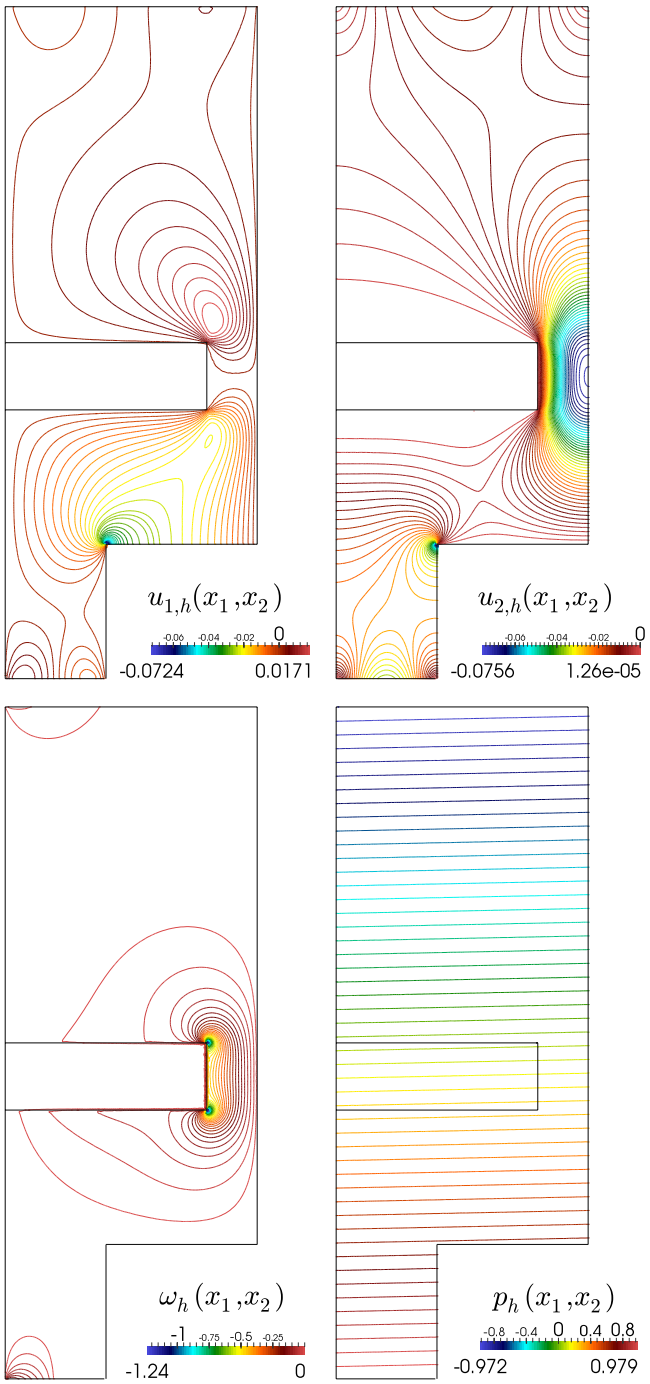

Figure 5.6: Example 4: Contour plots of the approximated velocity components (top), vorticity and pressure (bottom left and right, respectively), computed with an augmented $\mathbf{BDM}_1 - P_1 - P_1$ family for the Brinkman problem on a contracting channel with porous obstacle.

[15] P.G. Ciarlet, *The Finite Element Method for Elliptic Problems*. North-Holland, Amsterdam, New York, Oxford, 1978.

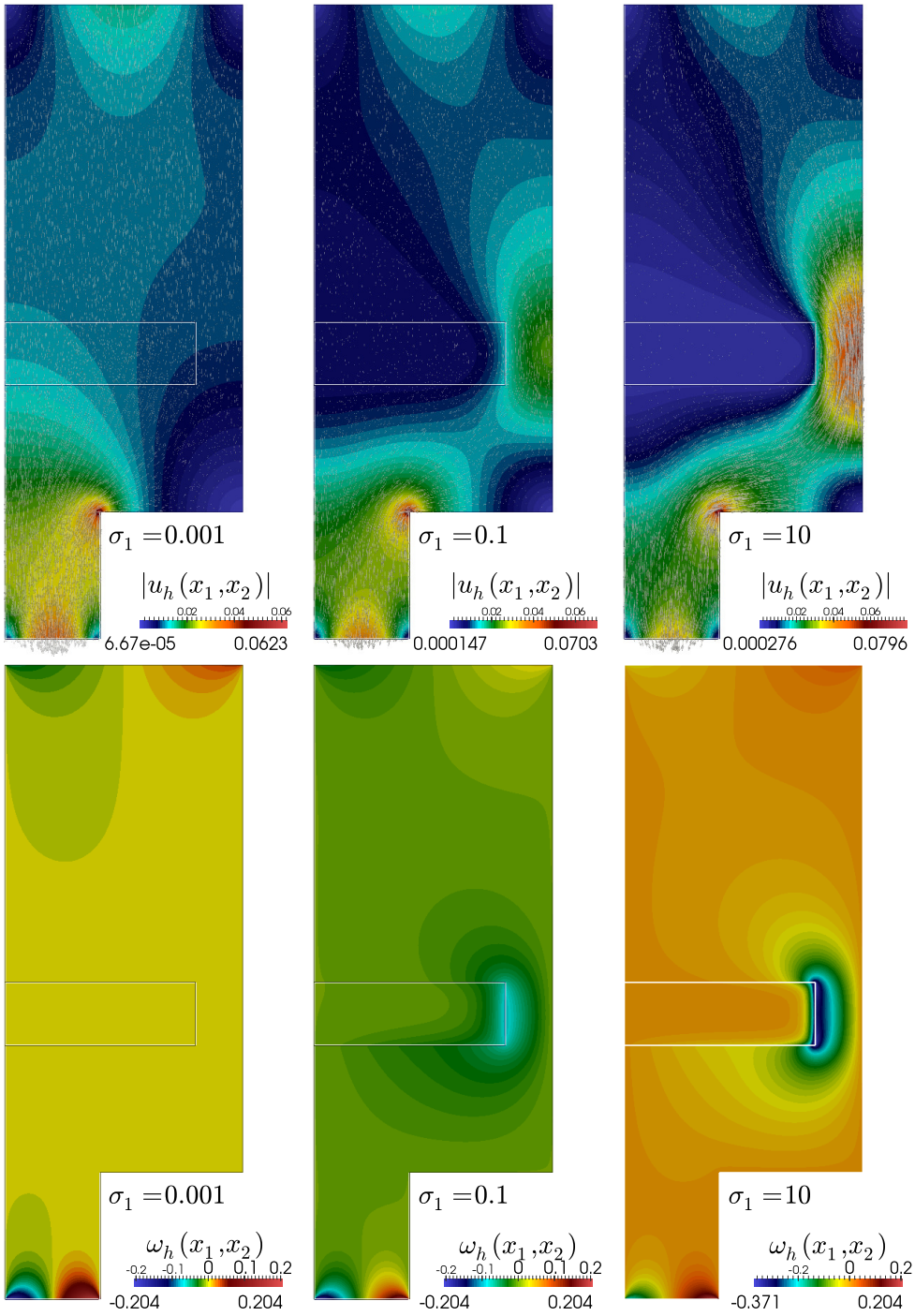

Figure 5.7: Example 4: Velocity magnitude with vector representation (top panels) and vorticity field (bottom panels) for different values of the inverse permeability σ_1 on the porous obstacle. Solutions were computed with an augmented $\mathbf{BDM}_1 - P_1 - P_1$ family on a contracting channel with porous obstacle.

[16] P. Clément, *Approximation by finite element functions using local regularisation.* RAIRO Modél. Math. Anal. Numér., 9 (1975) 77–84.

[17] B. Cockburn and J. Cui, *An analysis of HDG methods for the vorticity-velocity-pressure formulation of the Stokes problem in three dimensions*. Math. Comp., 81(279) (2012) 1355–1368.

[18] H.-Y. Duan, and G.-P. Liang, *On the velocity-pressure-vorticity least-squares mixed finite element method for the 3D Stokes equations*. SIAM J. Numer. Anal., 41(6) (2003) 2114–2130.

[19] F. Dubois, M. Salaün, and S. Salmon, *First vorticity-velocity-pressure numerical scheme for the Stokes problem*, Comput. Methods Appl. Mech. Engrg., 192(44–46) (2003) 4877–4907.

[20] L.E. Figueroa, G.N. Gatica, and N. Heuer, *A priori and a posteriori error analysis of an augmented mixed finite element method for incompressible fluid flows.* Comput. Methods Appl. Mech. Engrg., 198(2) (2008) 280–291.

[21] L.E. Figueroa, G.N. Gatica, and A. Márquez, *Augmented mixed finite element methods for the stationary Stokes equations.* SIAM J. Sci. Comput., 31(2) (2008) 1082–1119.

[22] L.P. Franca and T.J.R. Hughes, *Two classes of mixed finite element methods*. Comput. Methods Appl. Mech. Engrg., 69(1) (1988) 89–129.

[23] G.N. Gatica, *Solvability and Galerkin approximations of a class of nonlinear operator equations*. Z. Anal. Anwendungen, 21(3) (2002) 761–781.

[24] G.N. Gatica, *Analysis of a new augmented mixed finite element method for linear elasticity allowing* $\mathbb{RT}_0 - \mathbb{P}_1 - \mathbb{P}_0$ *approximations*. M2AN Math. Model. Numer. Anal., 40(1) (2006) 1–28.

[25] G.N. Gatica, *A Simple Introduction to the Mixed Finite Element Method. Theory and Applications*. Springer Briefs in Mathematics, Springer, Cham Heidelberg New York Dordrecht London, 2014.

[26] G.N. Gatica, L.F. Gatica, and A. Márquez, *Augmented mixed finite element methods for a vorticity-based velocity–pressure–stress formulation of the Stokes problem in 2D*. Internat. J. Numer. Methods Fluids, 67(4) (2011) 450–477.

[27] G.N. Gatica, L.F. Gatica, and A. Márquez, *Analysis of a pseudostress-based mixed finite element method for the Brinkman model of porous media flow*. Numer. Math., 126(4) (2014) 635–377.

[28] G.N. Gatica, N. Heuer, and S. Meddahi, *On the numerical analysis of nonlinear two-fold saddle point problems*. IMA J. Numer. Anal., 23(2) (2003) 301–330.

[29] G.N. Gatica, A. Márquez, R. Oyarzúa, and R. Rebolledo, *Analysis of an augmented fully-mixed approach for the coupling of quasi-Newtonian fluids and porous media*. Comput. Methods Appl. Mech. Engrg., 270(1) (2014) 76–112.

[30] G.N. Gatica, A. Márquez, and M.A. Sánchez, *Analysis of a velocity-pressure-pseudostress formulation for the stationary Stokes equations*. Comput. Methods Appl. Mech. Engrg., 199(17-20) (2010) 1064–1079.

[31] G.N. Gatica, A. Márquez, and M.A. Sánchez, *A priori and a posteriori error analyses of a velocity-pseudostress formulation for a class of quasi-Newtonian Stokes flows*. Comput. Methods Appl. Mech. Engrg., 200(17-20) (2011) 1619–1636.

[32] G.N. Gatica, R. Ruiz-Baier, and G. Tierra, *A mixed finite element method for Darcy's equations with pressure dependent porosity*. Preprint 2014-06, Centro de Investigación en Ingeniería Matemática (CI^{2}MA), Universidad de Concepción, Concepción, Chile, (2014).

[33] V. Girault and P.A. Raviart, *Finite element methods for Navier-Stokes equations. Theory and algorithms*. Springer-Verlag, Berlin, 1986.

[34] T. Gornak, J.L. Guermond, O. Iliev, and P.D. Minev, *A direction splitting approach for incompressible Brinkman flow*. Int. J. Numer. Anal. Model. B, 4(1) (2013) 1–13.

[35] J.J. Heys, E. Lee, T.A. Manteuffel, S.F. McCormick, and J.W. Ruge, *Enhanced mass conservation in least-squares methods for Navier-Stokes equations*. SIAM J. Sci. Comput., 31 (2009) 2303–2321.

[36] J.S. Howell, *Approximation of generalized Stokes problems using dual-mixed finite elements without enrichment*. Internat. J. Numer. Methods Fluids, 67(2) (2011) 247–268.

[37] B. Jiang, *The least-squares finite element method. Theory and applications in computational fluid dynamics and electromagnetics*. Springer Verlag, Berlin, 1998.

[38] K.H. Karlsen and T.K. Karper, *Convergence of a mixed method for a semi-stationary compressible Stokes system*. Math. Comp., 80 (2011) 1459–1498.

[39] K. Nafa and A.J. Wathen, *Local projection stabilized Galerkin approximations for the generalized Stokes problem*. Comput. Methods Appl. Mech. Engrg., 198(5-8) (2009) 877–883.

[40] J.P. Pontaza and J.N. Reddy, *Spectral/hp least-squares finite element formulation for the Navier-Stokes equations*. J. Comput. Phys., 190(2) (2003) 523–549.

[41] M. Salaün and S. Salmon, *Low-order finite element method for the well-posed bidimensional Stokes problem*. IMA J. Numer. Anal., doi:10.1093/imanum/drt063 (in press).

[42] P.S. Vassilevski and U. Villa, *A mixed formulation for the Brinkman problem*. SIAM J. Numer. Anal., 52(1) (2014) 258–281.

[43] R. Verfürth, *A posteriori error estimation and adaptive mesh-refinement techniques*, J. Comput. Appl. Math. 50(1-3) (1994) 67–83.

[44] R. Verfürth, A Review of A-Posteriori Error Estimation and Adaptive Mesh-Refinement Techniques. John Wiley and Teubner Series. Advances in Numerical Mathematics 1996.